PRECIPITATION PREDICTION OVER THE TROPICS FROM A GLOBAL SPECTRAL MODEL

T.N. Krishnamurti
Department of Meteorology, Florida State University
Tallahassee, Florida 32306, USA

Summary: This paper describes the capabilities of the FSU global spectral model in the area of *precipitation forecasting* over the tropics. Results for the resolution T106 over the monsoon area and for resolution T170 from typhoon forecasts are highlighted. An example of a precipitation forecast from a very high resolution global model highlights detailed hurricane rainbands and suggests the need to further increase the resolution of global models. The cumulus parameterization is described in the Appendix of this paper.

1. INTRODUCTION

With the improvements in resolution, physical parameterization and data analysis techniques, global models have displayed considerable improvement of skill in recent years. Operational weather centers – the ECMWF, U.K. Meteorological office, the National Meteorological Center Washington and the Japan Meteorological Agency – have participated quite actively towards this progress. The most striking improvements in the medium range have been evident north of 30 N over the northern hemisphere. The lack of observations has been a major factor for the lower skill over the southern hemisphere and especially over the tropics.

The FSU global spectral model was basically developed as a research model, Pasch (1983) and Krishnamurti *et al.* (1984, 1989). The model is outlined in Appendix I. This model has been improved considerably in recent years in the areas of initialization and physical parameterization. The impact of resolution (and its corresponding orography) on the predictability of monsoon phenomenon, typhoons and explosive cyclogenesis have been addressed.

This paper examines the precipitation forecast from the FSU model over the tropical latitudes. The convective and the nonconvective components are included.

2. PREDICTION OF MONSOON RAINFALL

In order to assess the quality of monsoon rainfall prediction it is necessary to map the 'observed' distribution of rainfall. Although several future programs, such as TRMM, have been proposed to provide reliable measures of the observed rainfall rates, at the present time we need to rely on polar orbiting and geostationary satellite radiances and raingauge

based estimates. Arkin *et al.* (1989) have proposed a histogram method to stratify polar orbitor satellite brightness estimates to calibrate rainfall rates. This method appears to be fairly reliable for the estimates of monthly rainfall rates. However for the verification of daily rainfall for numerical weather prediction, methods based exclusively on satellite based brightness are not entirely satisfactory. Martin (1983) has developed regression methods to utilize the notion of anvil expansion, over tropical cloud clusters, to obtain rainfall estimates from IR brightness using geostationary satellite data sets. This appears to provide somewhat more reliable estimates for daily fields, however tropical radiance data from several geostationary satellites at intervals of every 15 to 30 minutes are required for these computations and these are usually not properly archived for research. Furthermore these types of data are not available for the operational stream in the near real time.

The present study confines itself to experiments from the 1979 data sets. We have utilized the FGGE IIc raingauge data archives for 1979 along with the satellite radiance data sets to develop a regression as a first guess followed by an objective analysis (of 1° latitude/1° longitude averaged raingauge data) to obtain a mapping of 24 hourly tropical rainfall amounts. These were done for the entire tropical belt for the winter and the summer monsoon periods. Basically this analysis, Krishnamurti *et al.* (1983a), preserves the 1° averaged raingauge values over the land areas; however over the oceanic areas the analysis is largely regression dependent and is found to underestimate the rainfall by as much as 100%. At the present time we have not been able to improve the oceanic rainfall over the tropics. For the verification of precipitation forecasts we shall use these data sets with the aforementioned limitations in perspective. The following is a list of experiments that were carried out at the resolution T106 for the summer monsoon FGGE period.

Starting Date

1.	May 6	12 UTC
2.	May 9	12 UTC
3.	May 11	0 UTC
4.	June 20	12 UTC
5.	July 1	12 UTC
6.	July 24	0 UTC
7.	July 27	12 UTC
8.	August 2	12 UTC

All of these experiments were run with the 12 layer version of the FSU model described in Appendix I. Perhaps some of the major areas of differences in our model and the one being run operationally at various centers are in the treatment of the surface layer physics,

the modified Kuo scheme for deep convection and in the initial analysis of the moisture field. By placing a second computational level above the earth's surface ($\sigma = 1$) at the level $\sigma = \sqrt{.99}$ we were able to enhance the evaporation over the tropical oceans, Krishnamurti et al. (1989a), Manobianco (1989). This has been shown to have a major impact on the prediction of tropical cyclones (hurricanes and typhoons) and explosive cyclogenesis off the North American east coast.

Improvements in cumulus parameterization came from the use of a modified version of the Kuo's scheme, Krishnamurti et al. (1983b, 1988). Here the moistening, heating and rainfall rates were optimized with respect to observations over the global tropical belt. This is based on a statistical regression method where the moisture and heat budget, following Yanai et al.. (1973), are carried out using the FGGE data sets (ECMWF analysis and the FGGE IIc raingauge data). Based on these 'observed' budgets it is possible to optimize the classical Kuo's scheme. Appendix II describes this method. A comparison of the classical Kuo (1965) scheme with the modified scheme was illustrated in reference to the prediction of the formation of the onset—vortex of the FGGE year, Krishnamurti (1984). The heating rates of the classical Kuo underestimate the heating, and the monsoon onset is not predicted. With the use of modified Kuo a realistic prediction of the life cycle of the monsoon onset—vortex was possible.

Another important factor for the improvement of this forecast was the use of envelope orography, Wallace et al. (1983). The humidity analysis, beyond what was available in the ECMWF's final III b data set, was felt necessary. There was a significant mismatch between the location of clouds, as inferred from satellite IR data in tropical moist and rain areas. The physical initialization process entails running a reverse Kuo—algorithm that provides a consistent humidity analysis for a given precipitation field.

3. PREDICTION OF MONSOON RAINFALL AT DIFFERENT RESOLUTIONS

A monsoon depression formed over the northern Bay of Bengal on July 29, 1979, around 1200 UTC. In the following three days this storm moved very slowly westwards and stayed inland close to the Orissa Coast (near 15N). The prediction as a function of increasing resolution exhibited a major improvement in the position of the depression. Fig. (1) shows the analysis at 850 mb for day 5, i.e. for August 1, 1979, 12 UTC. The observed storm may be seen over the northeastern coastal area of the Bay of Bengal. The black dots on this diagram show the position of the storm on day 5 for the different resolutions. At T21 this storm is located over southern India; with the increase in resolution (T31, T42, T63, T106 and T170), this storm is located successively northwards
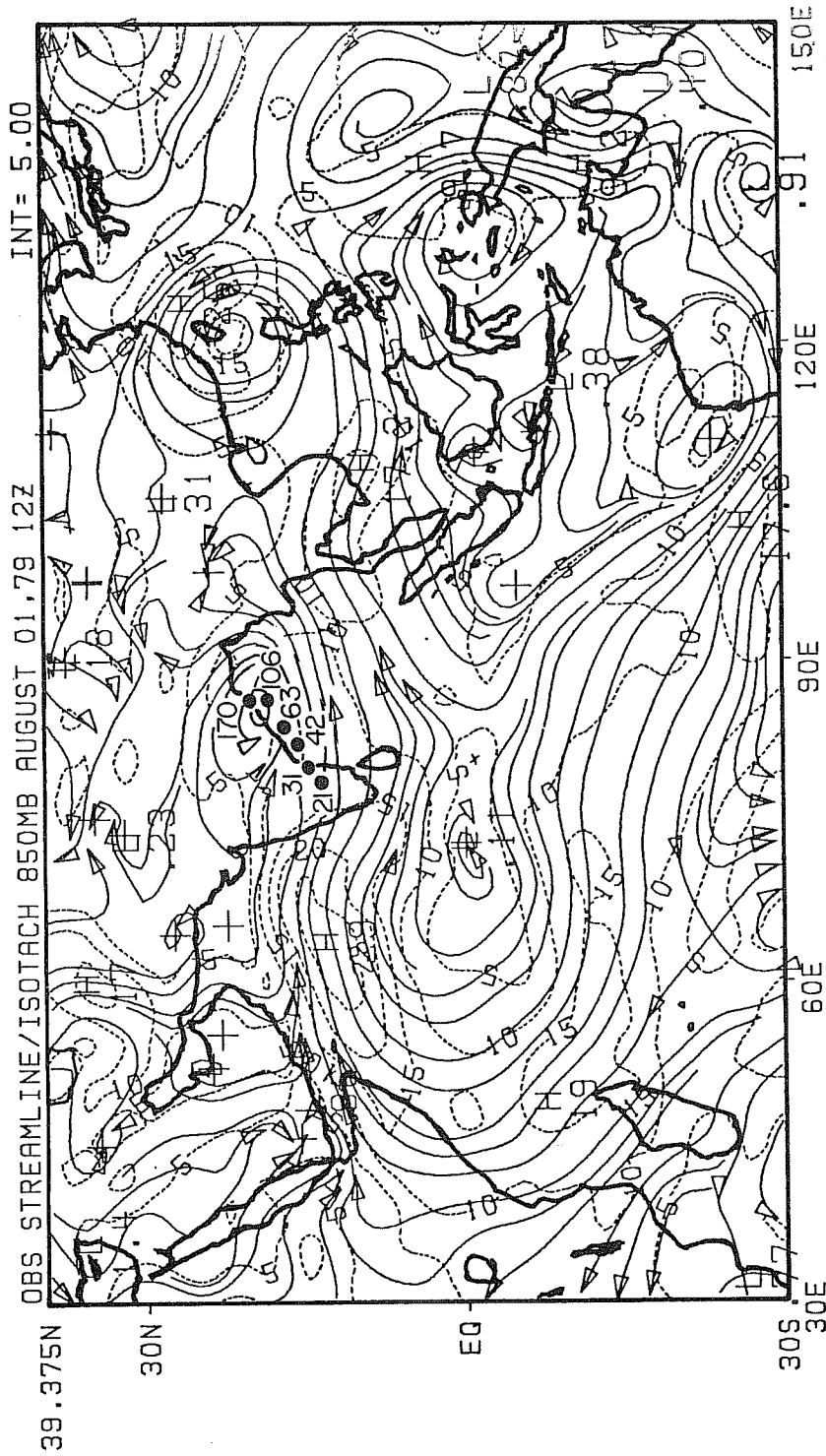
Fig. 1 850 mb flow field for August 1, 1979, 1200 UTC. Based on ECMWF's FGGE IIIb analysis (streamlines: solid line; isotachs: dashed lines, units ms^{-1}). The black dots denote the position of the center of the monsoon depression predicted by the global model at the resolutions T21, T31, T42, T63, T106 and T170.

to its correct position at T106 and T170. The position error is quite large at the resolution T21.

The position error of the monsoon depression at the different resolutions seems to be closely related to the forecast errors in the position of typhoon Hope over the western Pacific ocean. We view a broad scale differential heating as an important aspect for the strength and position of monsoon circulation over the Arabian Sea and India. In this situation the heat source is defined by the heavy precipitation of the typhoon, while the heat sink resides over the southern Indian ocean near the South African Coast; with the increase in resolution, the heat source moves to a more northerly position near Hong Kong. The zonal flow acceleration between the heat sink and the heat source occurs at a more southerly latitude (near 7 to 8N) at the resolution T21. On the cyclonic shear side of the lower tropospheric zonal westerly flow, a cyclone forms near 10N over southern India for T21. As the resolution is increased to T106 and T170 the zonal flow accelerations between the heat sink (over the Mascarene high) and heat source (typhoon Hope) occur much further north. A depression forms at the more correct position on the cyclonic shear side of this accelerating zonal flow. Thus we find that the resolution has a strong impact on the location of the typhoon and the broad scale monsoon current. Resolution errors are reflected in both of these features that seem to be interrelated. This typhoon is discussed in section 7.

The predicted flow field at 850 mb for day 3, as a function of spectral resolution, is shown in fig. 2. Here the results for the resolution T21, T31, T42, T63, T106 and T170 are shown. Of interest here is the location of the monsoon depression and its shift to a proper location with increasing resolution. The circulations were best described on day 3 at the resolution T106 and T170. When we examined the velocity potential χ, fig. 3, at the 200 mb for day 3, we noted that a divergent outflow center is located over southern India for T21; as the resolution is increased to T170 this splits into two outflow centers. The northern one moves over the correct location of the Bay of Bengal depression while the southern center moves over the Arabian sea. These shifts are of the order of 1,000 km and show a significant impact of resolution on the forecasts. The three day accumulated precipitation as a function of resolution is shown in fig. 4. During this time most of the heavy rain occurred over the Arabian sea coast of western India and the central Bay of Bengal. This feature was resolved by the model at T63, T106 and T170. At the resolution T21 the heaviest rainfall occurred over southern India. The heaviest accumulated 3 day rainfall amounts over the depression for the resolutions T21 through T170 were 154, 190, 182, 198, 336 and 221 mm/3 days respectively.
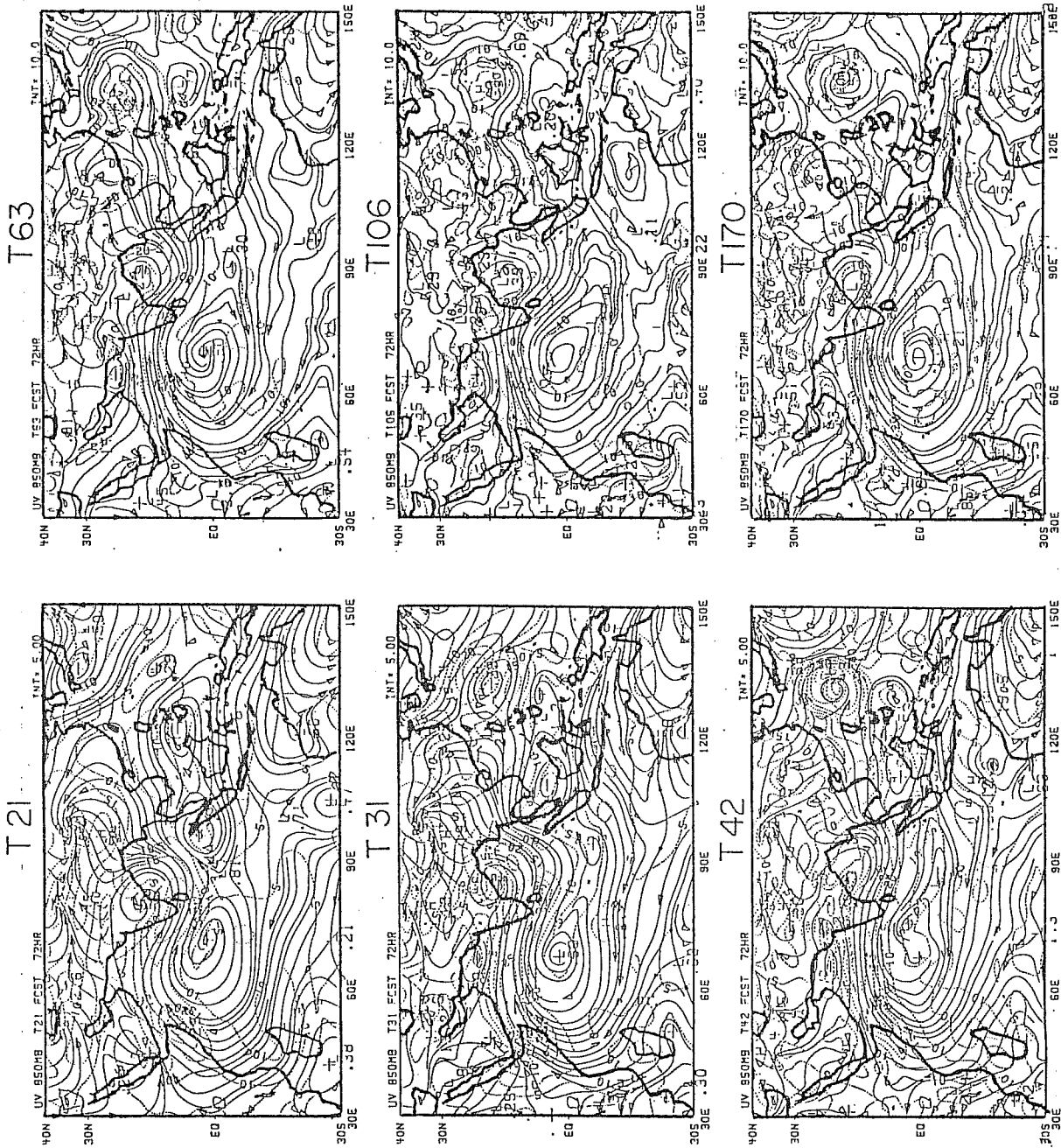
Fig. 2 Predicted 850 mb flow field (streamlines: solid lines; isotachs: dashed lines, units ms⁻¹) at different resolutions of the global model on day 3.
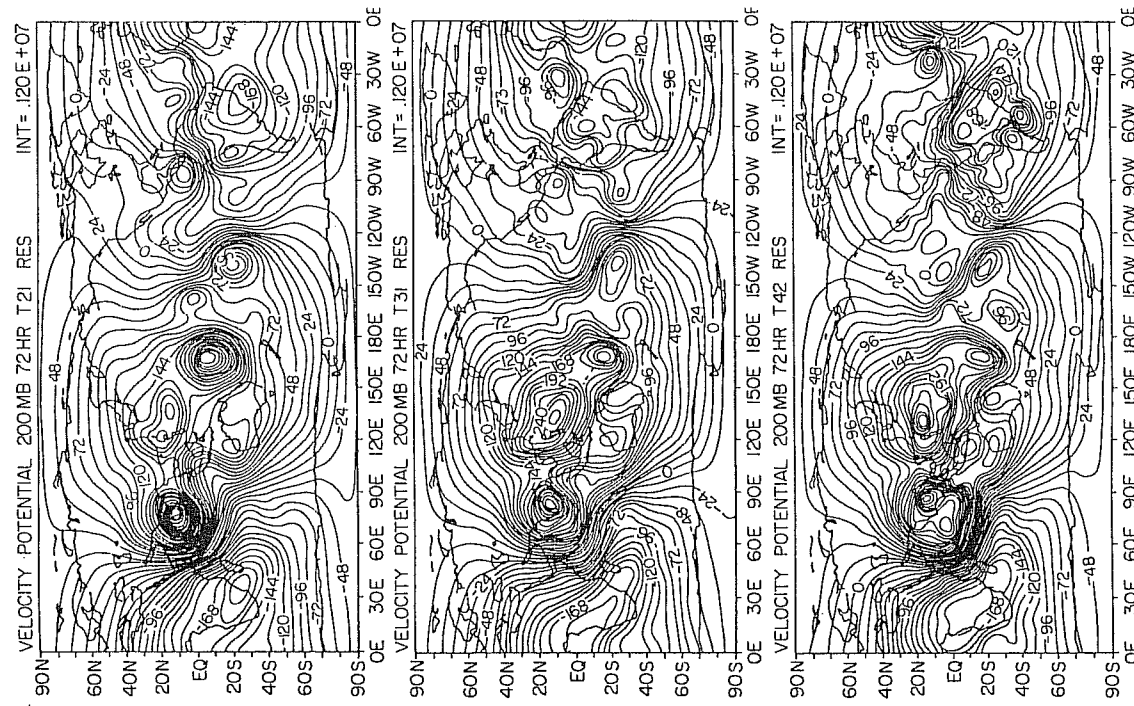
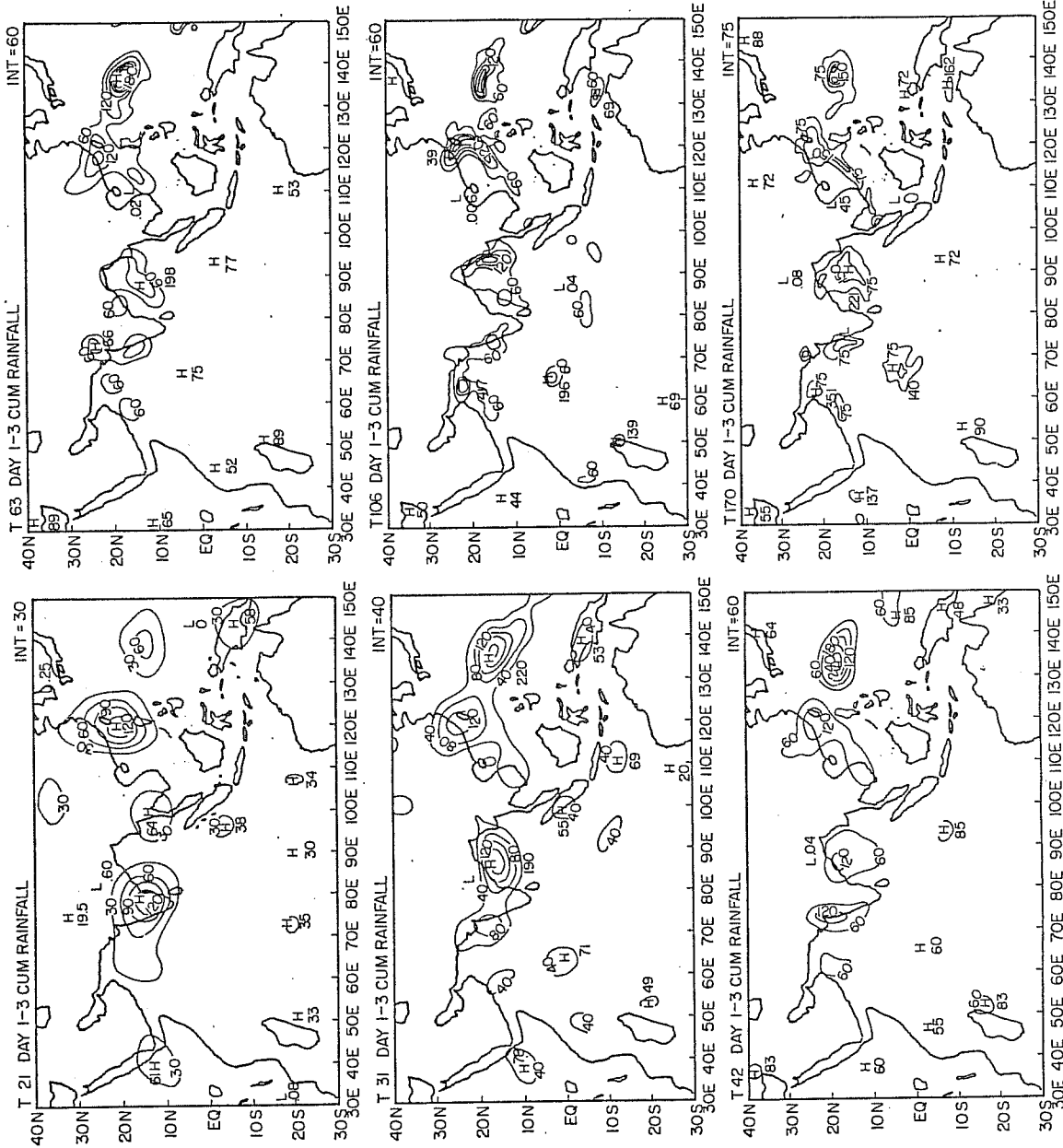Fig. 3 Predicted velocity potential at 200 mb on day 3 of forecast. Interval of analysis 10 m²s-1.

Fig. 4 Three day accumulated rainfall (mm/3 days) from the prediction at different resolutions T21 through T170. The day 0 for this experiment is July 27, 1979, 12 UTC.

4. ENSEMBLE AVERAGE DAY 1, 2, 3, AND 6 DAY PREDICTIONS OF MONSOON RAINFALL (T106)

Here we shall show the skill of monsoon rainfall predictions of the FSU model at the resolution T106 from ensemble averages of days 1, 2, 3, and 6 of forecast. The ensemble is based on 8 experiments during the northern summer of 1979. In the following diagrams (fig. 5 a through e), the left panels show an ensemble based on observations, while the right panels show the predictions. Fig. 5a shows the ensemble average of one day forecast and the corresponding observations. All rainfall rates are expressed in the units mm/day. As stated earlier the oceanic estimates of the observed rainfall are too low and invariably the model predictions over the ocean are larger in comparison. The ensemble of 1, 2, and 3 day rainfall shows a zonally oriented band of precipitation centered along roughly 15N. Heavy precipitation occurs along the west coast of India, the Burmese coast of the Bay of Bengal, the Philippine sea and the western Pacific ocean. The model estimates, although substantially larger over the ocean, are in close agreement with respect to the position of the rainfall belt.

The ensemble of the day 3 of 'observed estimates' compared to predictions does not show any particular bias or growth of systematic errors. The land areas were relatively dry with rainfall amounts less than 10 mm/day; that feature was handled quite well in the day 3 forecasts. In panels 'd' and 'e' of fig. 5 we show the 3 and 6 day average rainfall amounts for the same 8 experiments. The ensemble of 3 day averaged (i.e. sum of days 1, 2, and 3) rainfall shows a close agreement in the position of the belt over the eastern Arabian sea, the eastern Bay of Bengal, the Philippine sea and the western Pacific ocean. It is of particular interest to examine the 6 day ensemble average rainfall (fig. 5e). The comparison of the 'observed' and the model predicted amounts are quite striking. A narrow zonal belt of rainfall along central India separates the heavier rainfall over the Arabian sea and the Bay of Bengal. All of these features are reasonably handled by the model. Similarly the 6 day averaged rainfall over the western Pacific ocean is quite reasonably predicted by the model. The model predictions do not match the observation near the Persian Gulf and the southern Bay of Bengal. These may be related to deficiencies in the initial wind analysis and the definition of sea surface temperatures. The predicted Somali jet at T106 was somewhat stronger and was located a few degrees north of the observed position. The cyclonic shear side of the jet was also displaced somewhat farther north over the Arabian sea where the model predicted excessive convection. This discrepancy may also be related to the deficiencies of the regression method for 'observed' rainfall analysis, since it systematically underestimated rainfall over the oceans.
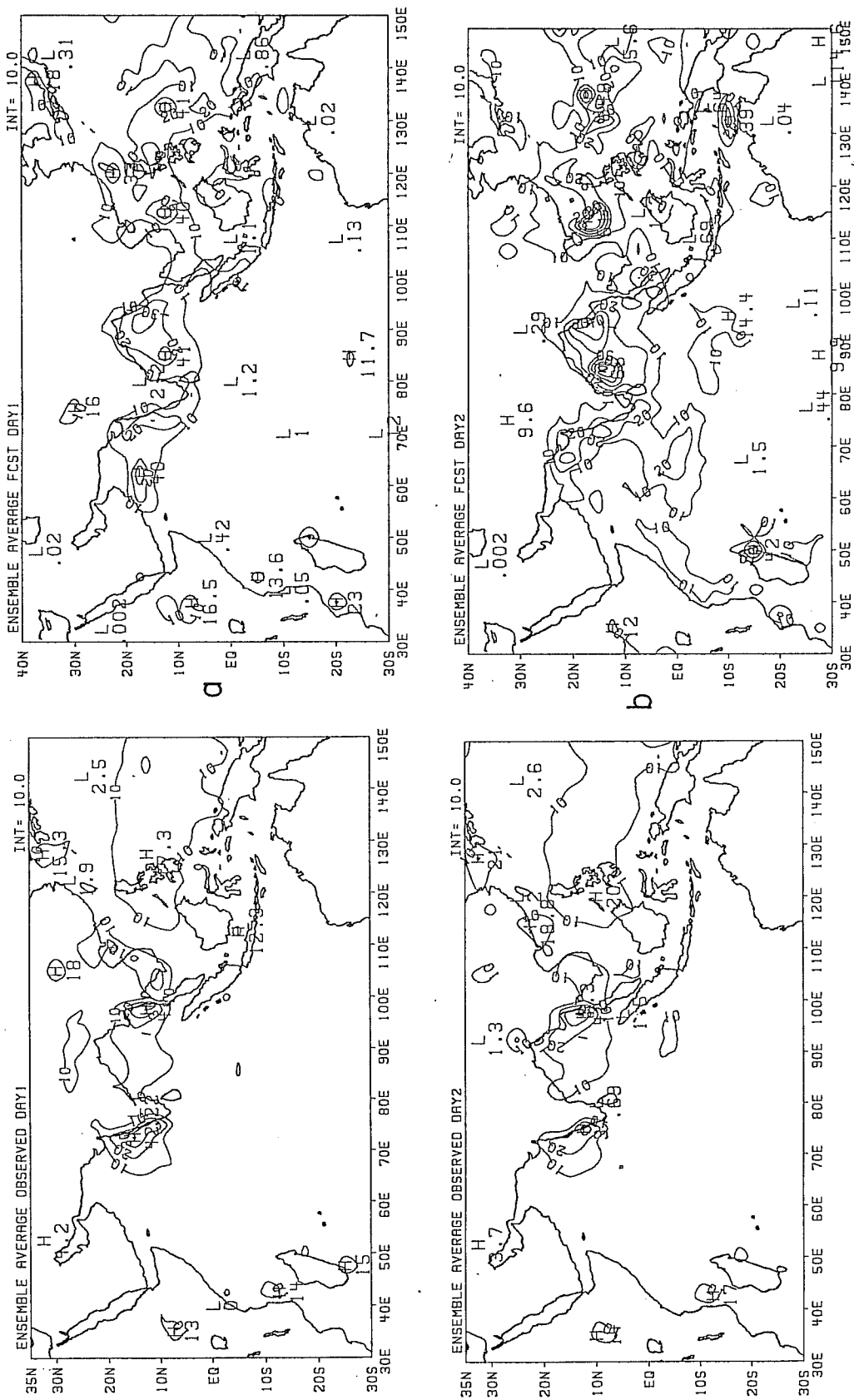
Fig. 5a Left panel shows the ensemble average of day 1 'observed' rainfall for 8 experiments. The right panels shows the ensemble average of day 1 predicted rainfall for 8 experiments.
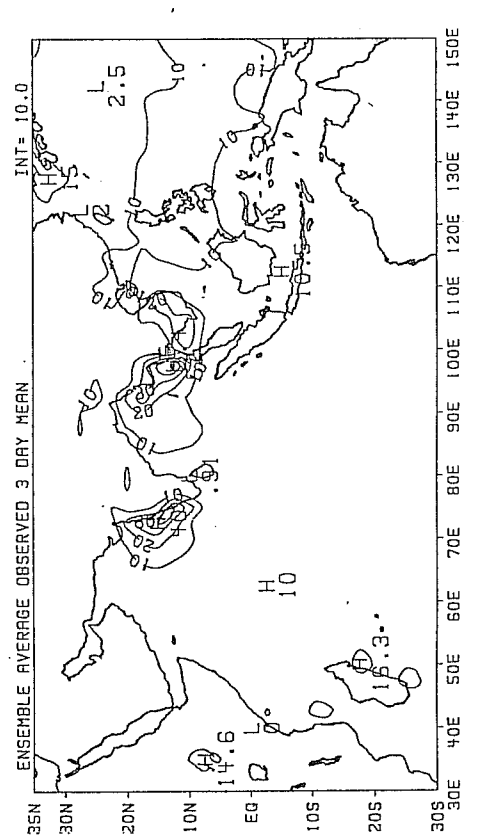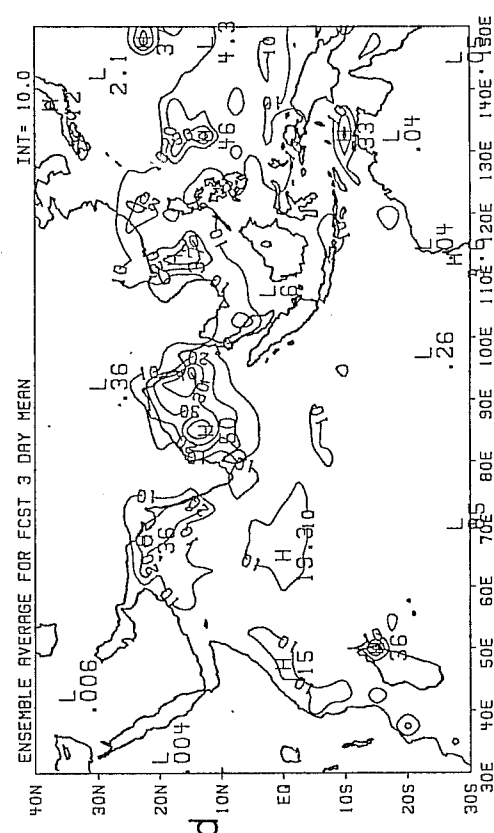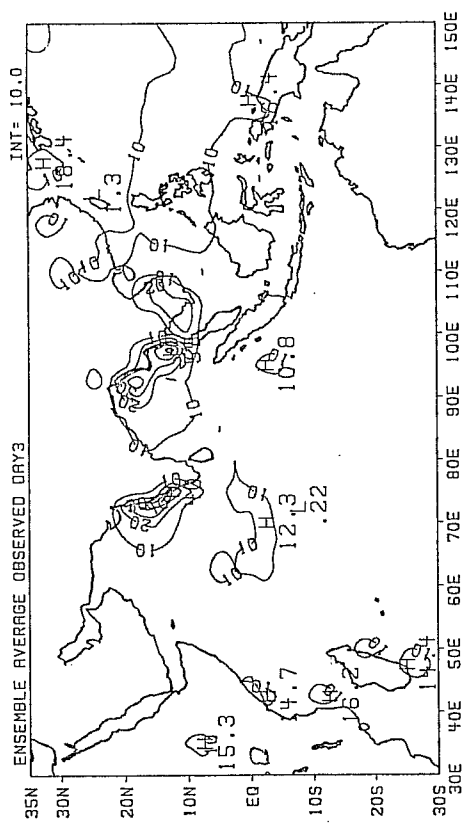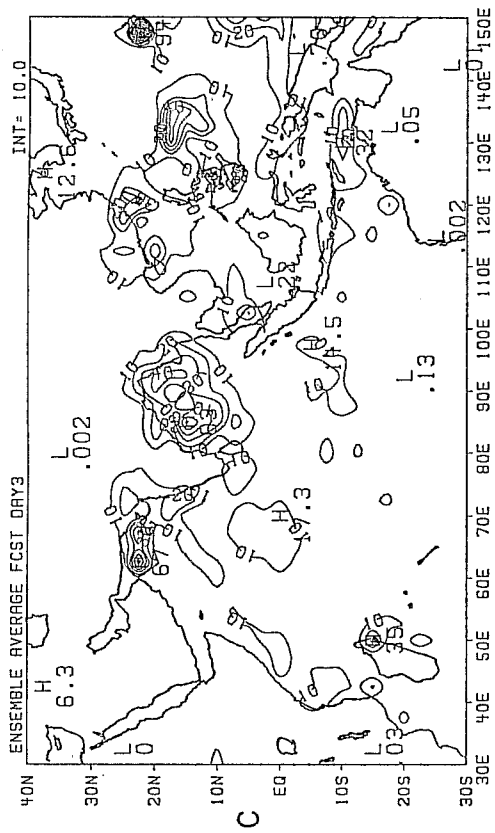
Fig. 5b Same as fig. 5a for day 2.

Fig. 5c Same as fig. 5a for day 3.

Fig. 5d Averaged precipitation for day 0 to day 3; left panel based on observations, right panel based on forecasts.
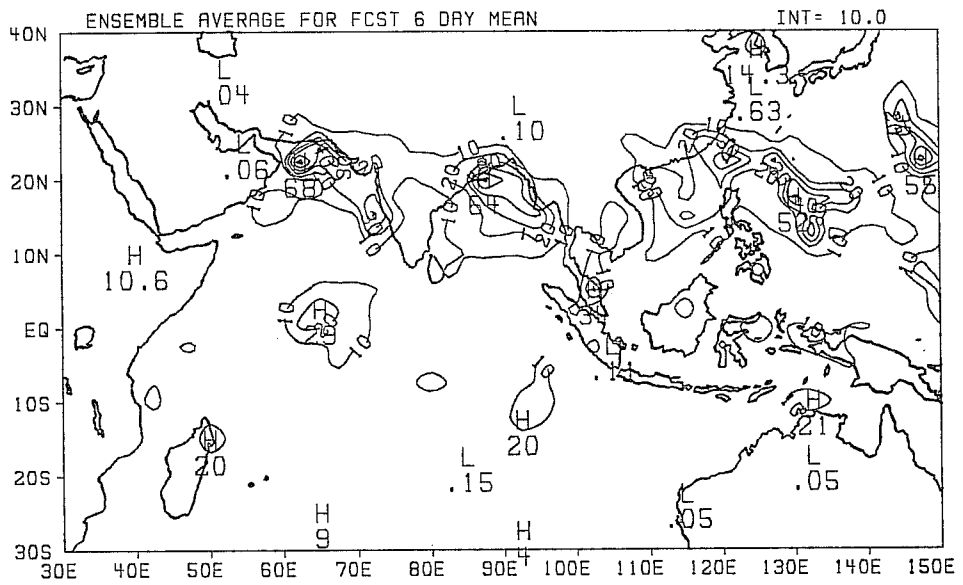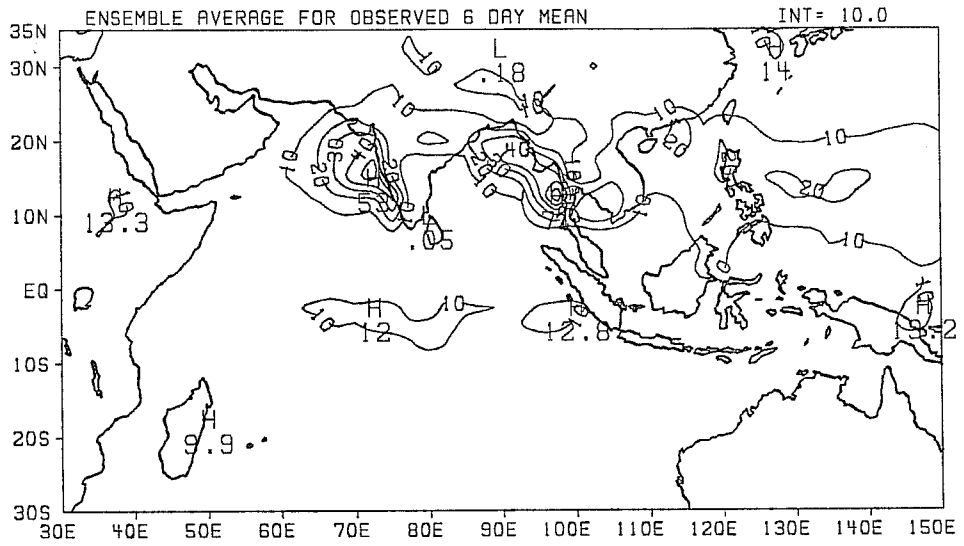
Fig. 5e Same as fig. 5d for day 0 to day 6.

Overall the predicted 6 day averaged rainfall over the monsoon region appears quite impressive for the 8 cases that were run at the resolution T106. It appears that, *given the FGGE quality data sets*, monsoon rainfall can be predicted for a period of about one week. We have not examined the forecasts beyond one week since not many cases were run for that long a period.

5. TROPICAL CYCLONE RAINBANDS

In this section we shall show a comparison of experiments on tropical cyclone rainfall from T106 as compared to results from a very high resolution regional model.

Using a sophisticated high resolution regional model (horizontal resolution of the order of 45 km) and updated real data 'perfect' boundary conditions, the prediction of the landfall of a tropical cyclone was carried out to 72 hours. The detailed rainbands simulated by the model's precipitation were in close agreement to detailed bands seen from satellite photographs. A number of sensitivity experiments were carried out. The starting date for the series of experiments was May 11, 1979, 00 UTC. The experiments utilized a domain roughly between 45E and 115E longitude and 8S to 40N latitude. The following is a list of experiments that were carried out.

- Regional model forecasts at a horizontal resolution of 1.875°.
- Regional model forecasts at a horizontal resolution of 0.938°.
- Regional model forecasts at a resolution of 0.469°.
- Global model forecasts at a resolution T106.

Furthermore, regional model forecasts at the resolution 0.469° were carried out with the following options:

- Perfect boundary conditions with an improved parameterization of the ground wetness.
- Perfect boundary conditions with a simple formulation of the ground wetness.
- Boundary conditions obtained from T106 forecasts with the improved parameterization of the ground wetness.
- Time invariant boundary conditions.

The details of these experiments are described in Dastoor and Krishnamurti (1989). The FSU regional model is described in Krishnamurti *et al.* (1989b). Here we shall summarize the main findings of the study that are relevant to the issues of tropical rainfall prediction.

The parameterization of ground wetness was a simple function of a prescribed surface albedo field and the surface relative humidity. The more sophisticated parameterization of the ground wetness was based on the following procedure.

- Following Luo and Yanai (1984) we carried out daily budgets of heat and

moisture, i.e. Q_1 and Q_2 based on the ECMWF FGGE IIIb data sets.

- We calculated the vertical distribution of the rate of radiative heating Q_R from our radiation algorithms.

- From the vertical integrals of Q_2 and $Q_1-Q_2-Q_R$ we determined the surface fluxes of latent and sensible heat following Yanai *et al.* (1973).

- Thus we generated a data set for the summer season, i.e. the surface fluxes over the tropics.

- Using the surface similarity theory as a framework we deduced a ground wetness parameter consistent with the latent heat fluxes. A data base for the ground wetness was generated for the summer months. Given the surface fluxes, a data base for the ground temperature was also prepared using the surface energy balance.

- The above ground wetness was next regressed as a function of the past 24 hour rainfall, soil indices, surface albedo, ground temperature and relative humidity.

- This regression determines a parameterization for the ground wetness in the prediction model.

Surface fluxes based on this parameterization at t = 0 match closely those deduced from diagnostic budgets of Q_1 and Q_2. In contrast, the fluxes implied by the simpler formulation of ground wetness show a poor agreement.

In reference to realistic simulation of rainbands the following results were obtained from the above experiments.

- The time invariant boundary conditions, based on the initial boundary values, failed to produce realistic bands. The forecasts of the fields had the largest errors.

- The best results on the simulation were obtained when the so called 'perfect boundary conditions' were used with the improved parameterization of ground wetness. Although the simpler parameterization does not distort the rainbands, it contributed to a slightly slower phase speed of the tropical cyclone. That was a consequence of drier soil conditions in the simpler parameterization of ground wetness which did not take into account the past rainfall. The slightly increased phase speed (100 km/day) from the improved parameterization places the bands over the land area of southern India in much closer agreement to those seen in the satellite imagery and the raingauge records. Figs. 6a and b illustrate the rainbands as seen from the DMSP satellite for hours 12 and 36. The best results are shown in figs. 7a and b. These show the banded structure of the rainfall totals (mm/day) for
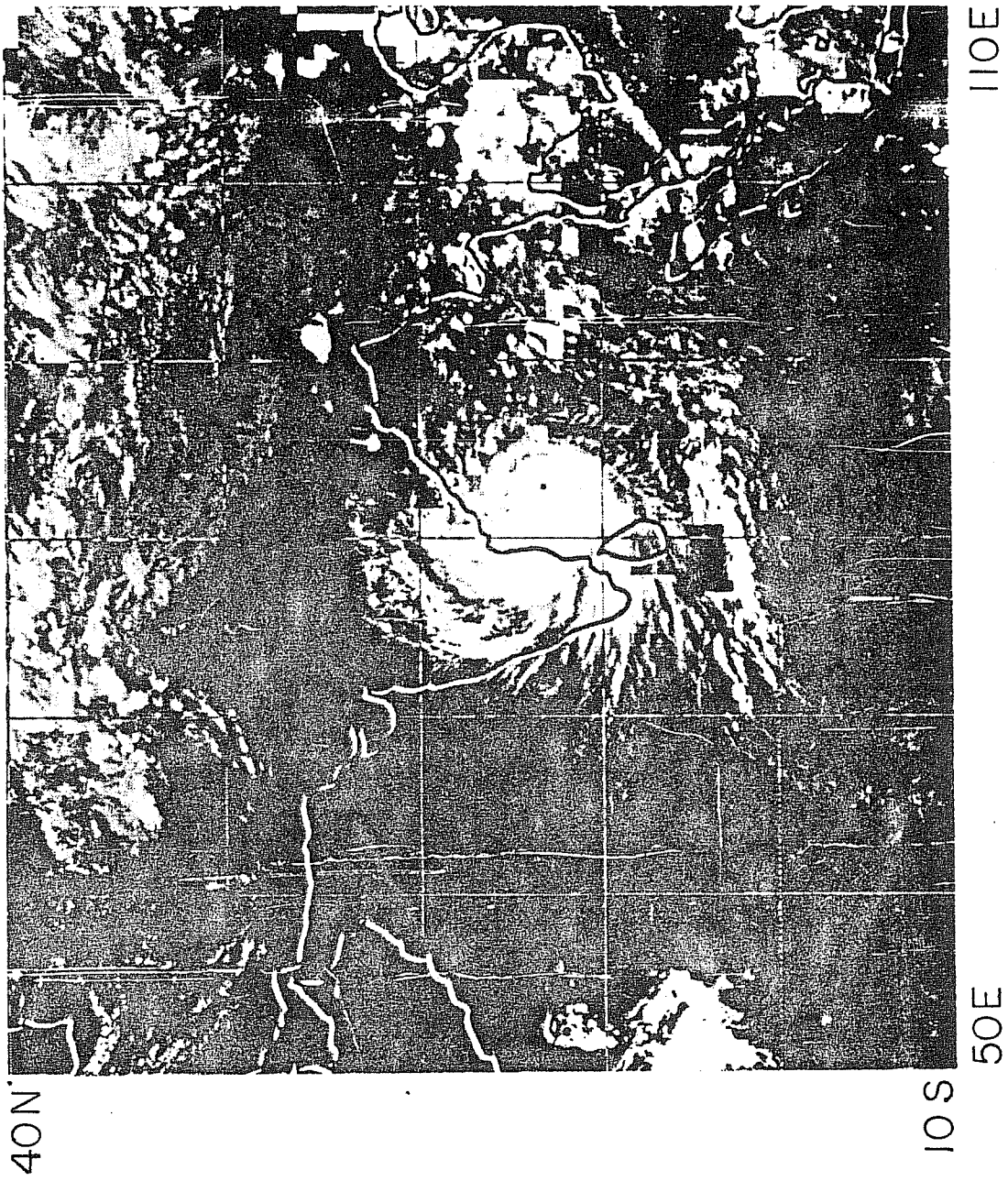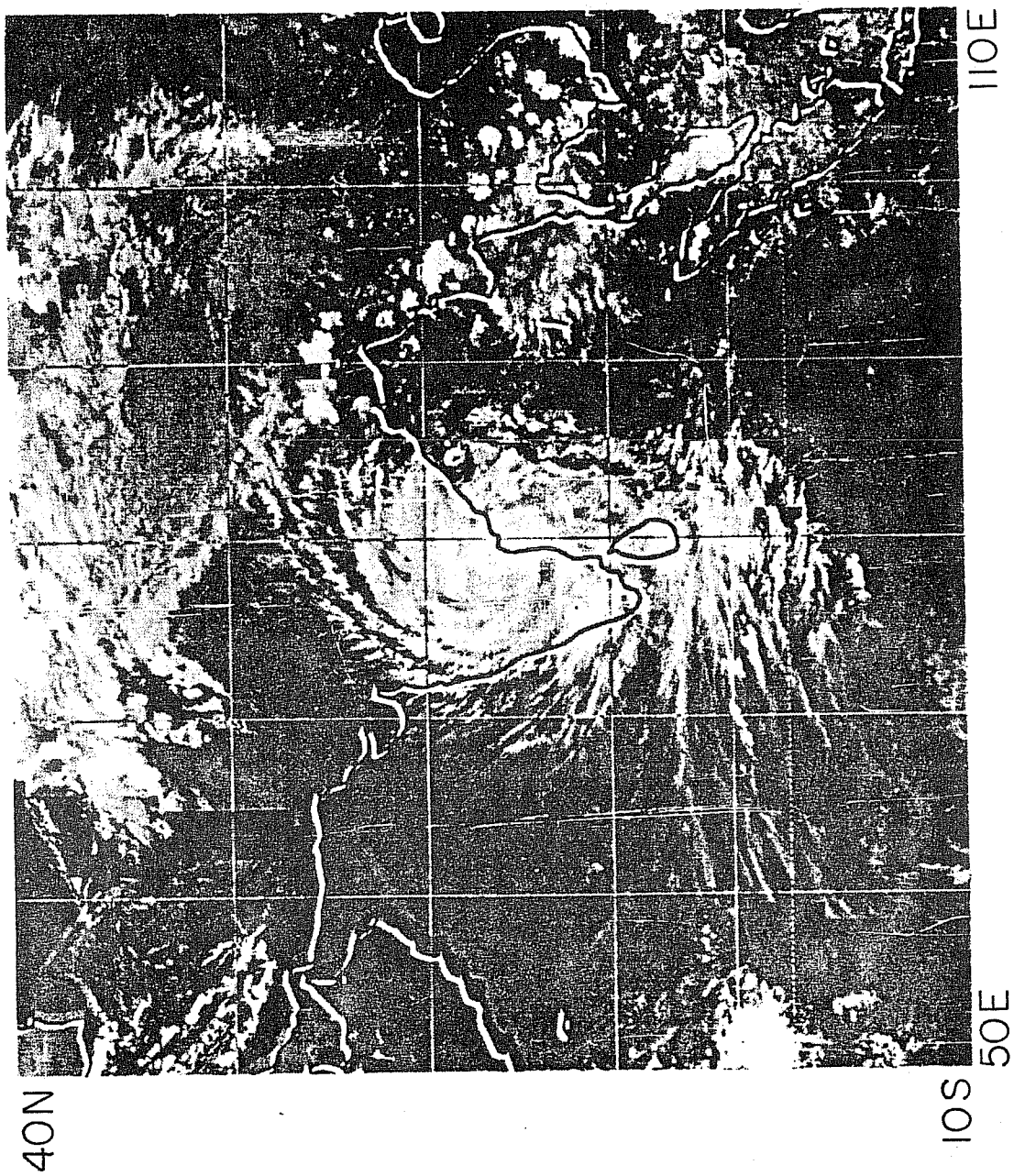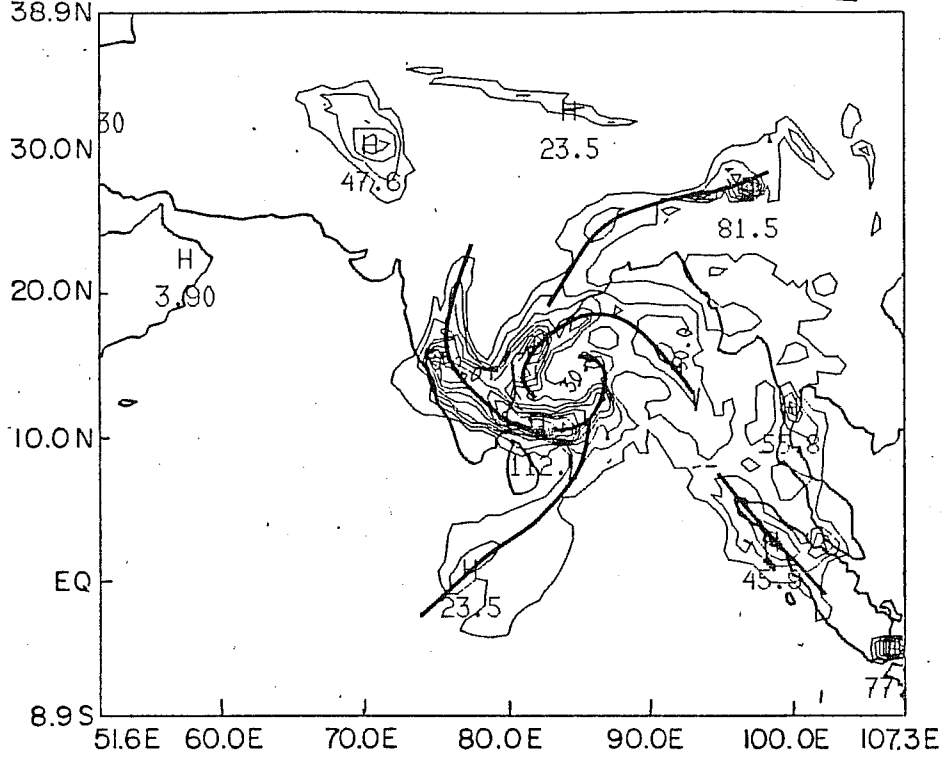
Fig. 6a Satellite imagery (DMSP); May 11, 1979, 12 UTC
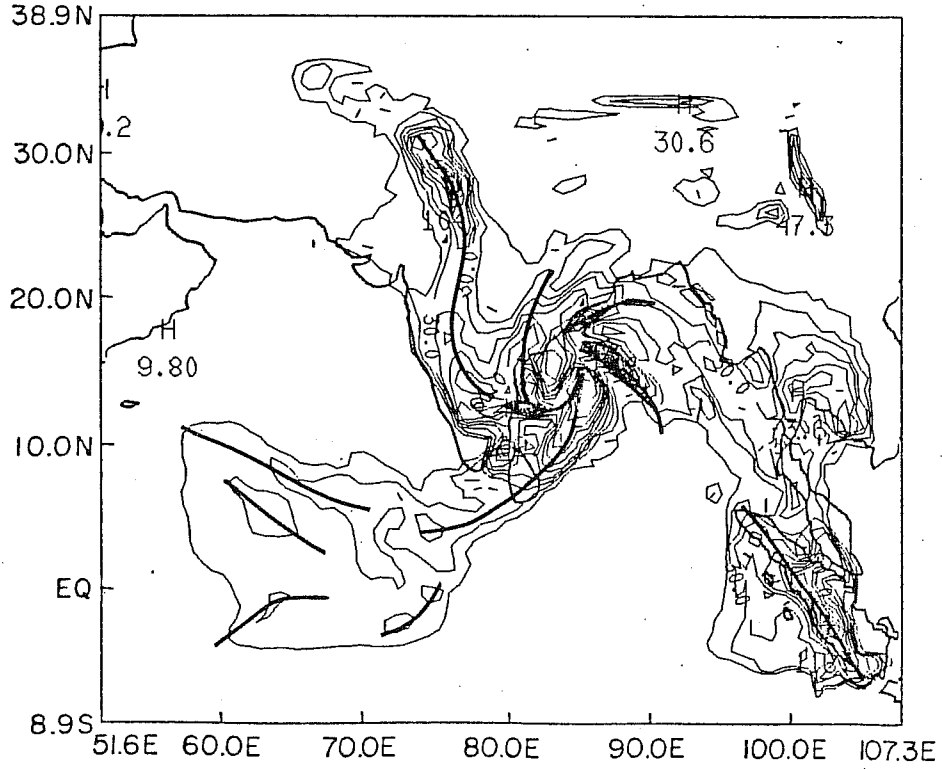
Fig. 6b Satellite imagery (DMSP); May 12, 1979, 12 UTC

a

b

Fig. 7a Predicted rainfall hours 0 to 24, mm/day.

Fig. 7b Predicted rainfall hours 24 to 48, mm/day.

hours 0 to 24 and hours 24 to 48 respectively. The satellite imagery is roughly centered in time with respect to these rainfall rates. In this experiment when the resolution was decreased to 0.938° and 1.875° the bands deteriorated. The T106 global forecasts simulate a rain belt in the correct position but fail to show banded structure. That was also true for the regional model at the highest resolution when the boundary conditions from the global forecast at T106 were used.

Basically we have learned that much higher resolution and improved surface processes are needed to describe the tropical cyclone during its landfall. The boundary condition problem for the regional model remains unsolved at the present time. The use of perfect boundary conditions provides much superior simulation when compared to the use of high resolution (T106) boundary conditions from a global model. The resolution of the transform grid at T106 is around 100 km while the regional model resolution was around 45 km. This raises the possibility that we might be better off using a global model at resolutions such as T230 and avoid lateral boundary conditions. This would require formidable computations with presently available computers but seems necessary because of the importance of the hurricane landfall problem.

Not mentioned in the discussion above is the issue of data sets. We have worked with the final FGGE IIIb analysis produced by the ECMWF. Their product for the global experiment includes a four dimensional data assimilation followed by a multivariate optimal interpolation. The quality of the delayed data from the global experiment does seem quite impressive. The results, in general, were quite poor when we used operational data sets, Krishnamurti *et al.* (1989a).

6. RAINFALL PREDICITON – EASTERLY WAVES

In a recent analysis on the performance of the ECMWF's operational model (run at T106), Reed *et al.* (1987, 1988) examined the prediction over the west African – tropical Atlantic regions. They noted that the analysis captures the basic structure of the African and the tropical waves. The prediction up to days 2 and 3 resolves the horizontal flow field quite accurately. However, they concluded that the precipitation forecasts do not agree with observations even at days 2 and 3.

We have examined numerous examples of developing and non–developing easterly waves for the FGGE period utilizing the FSU T106 predictions. The data coverage during the FGGE period includes the 2 to 3 years of delayed collection of marine, WWW, commercial aircraft and cloud winds; this coverage is somewhat superior to the

operational real time data coverage of the middle 1980's that were used by Reed *et al.* (1987, 1988). The current operational data coverage is equally poor over west Africa, Bengtsson and Shukla (1988).

Our results, with the FGGE data, in general show that African waves can be tracked across the Atlantic ocean for time periods of the order of 4 to 6 days. The circulation forecasts are remarkably good on this time scale. Some of the forecasts are excellent even on the medium range time frame of 6 to 7 days. Here a typical example of an African wave prediction at T106 is illustrated that shows a remarkable prediction of the rainfall following the wave to 72 hours. The passage of this wave was reasonably predicted through day 6 of the forecast.

Here we shall consider a three day period starting on August 30, 1979, 12GMT. The observed and the predicted wind fields at 850 mb over this domain for day 1, 2 and 3 of forecasts are shown in fig. 8. The panels 5 a, b, c and d show the 0, 24, 48 and 72 hour prediction. The trough line of the observed and the predicted waves are identified by a heavy dark line. The prediction of the vortex to the north of Venezuela is handled extremely well by the model (at the resolution T106). Two other easterly waves near 55W and 10W are reasonably handled by the model. The phase speed of the latter was somewhat too fast compared to the analysis at 48 hours. The major disturbance that is located near 70–75W eventually became hurricane Frederick by day 3 of forecast, Krishnamurti *et al.* (1989a).

Fig. 9 illustrates the rainfall prediction at the resolution T106. As stated earlier, the 'observed' rainfall amounts, based on regression methods over the ocean are highly underestimated. The discrepancy is evident for three of the Atlantic waves. Between hours 24 to 48 the 'observed maximum rainfall' for the three waves were around 34, 27 and 10 mm/day. The corresponding predicted values are 70, 38 and 108 mm/day. The frontal rain along the east coast of North America was also mostly convective. These oceanic rainfall amounts were also not adequately described by the satellite regression; however, the predicted axis closely corresponds to a sharp cloud line that was discerned in the satellite photograph for September 1, 1989 (hour 48). The resolution of the basic IR data, 2.5° latitude/2.5° longitude, did not adequately resolve this feature. Heavy rainfall amounts around 23 mm/day over the land areas of South Florida were based on raingauge observations. The model predicted value over the region was of the order of 32 mm/day.
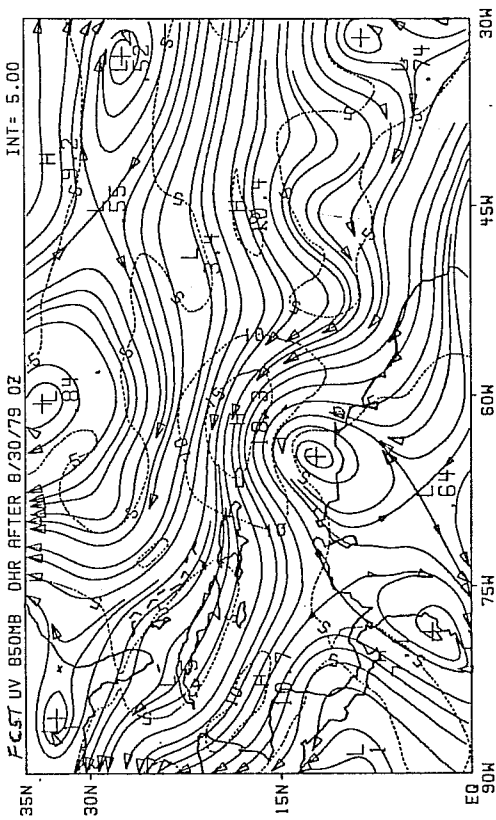
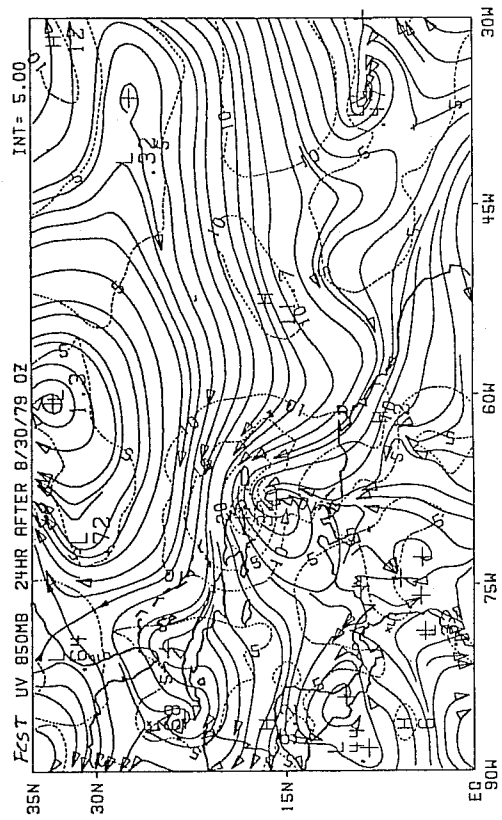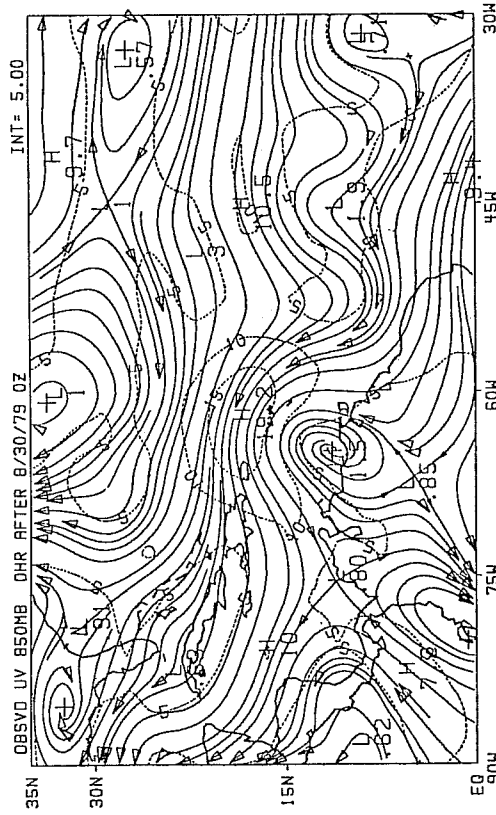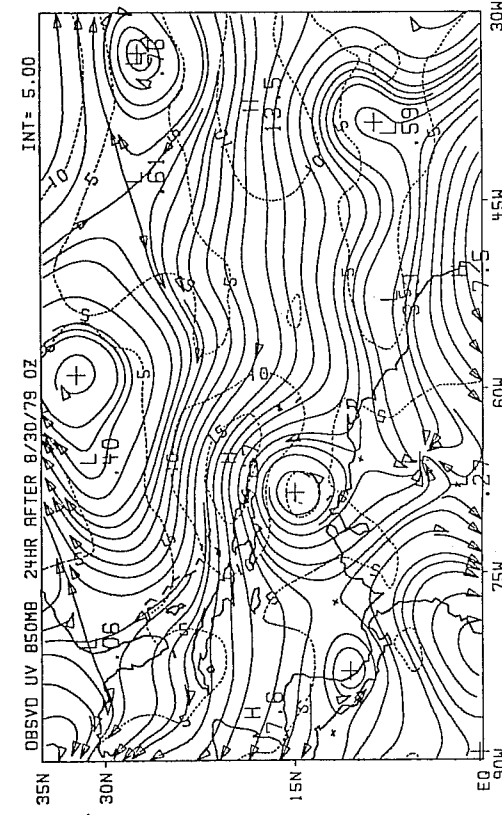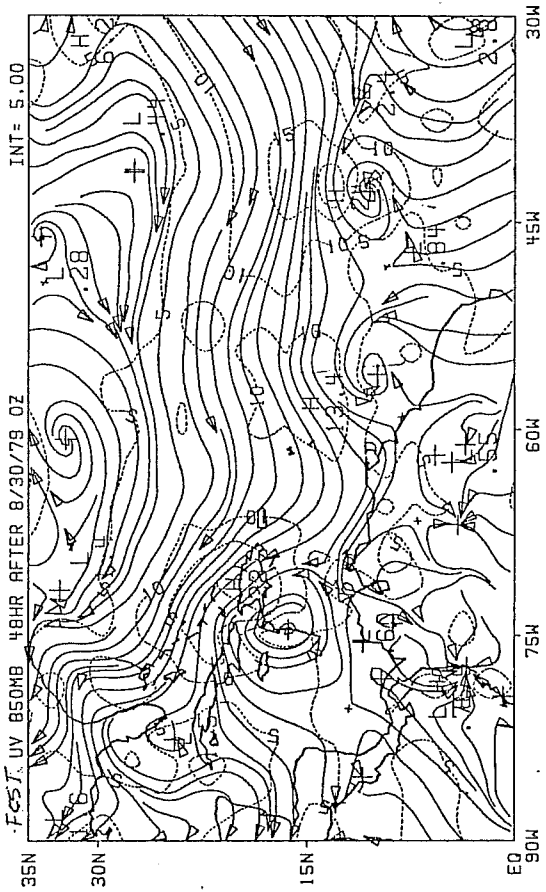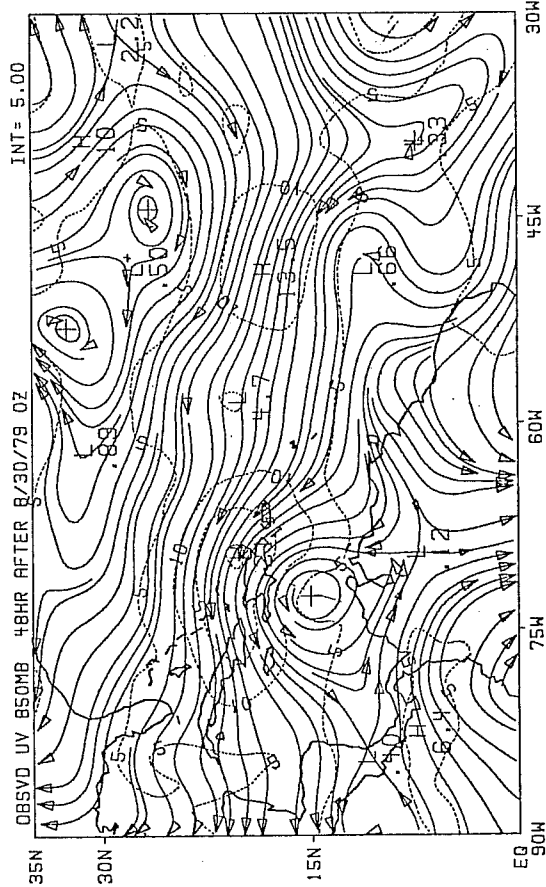Fig. 8a, b, c These diagrams, respectively, show the observed (left) and the predicted (right) wind fields for hours 0, 24, 48 and 72 for a global model run (T106). t = 0 is at 12 UTC on August 30, 1979.
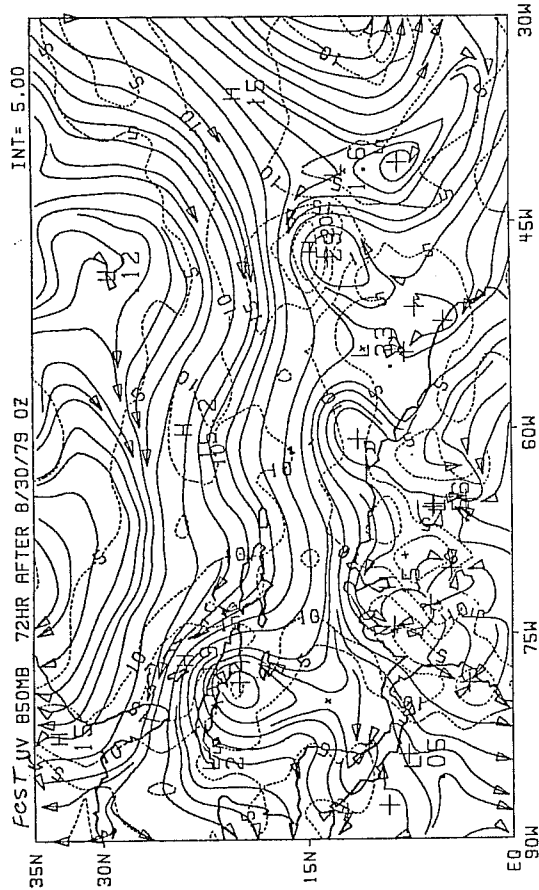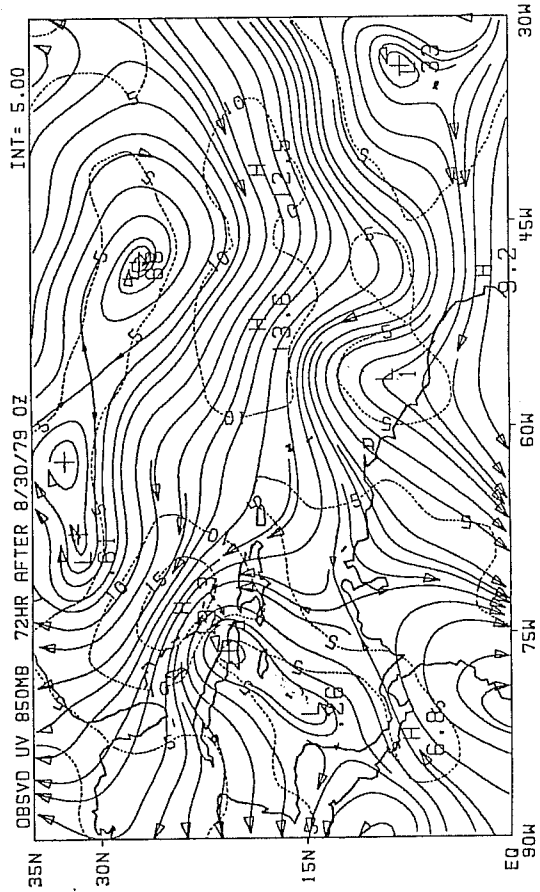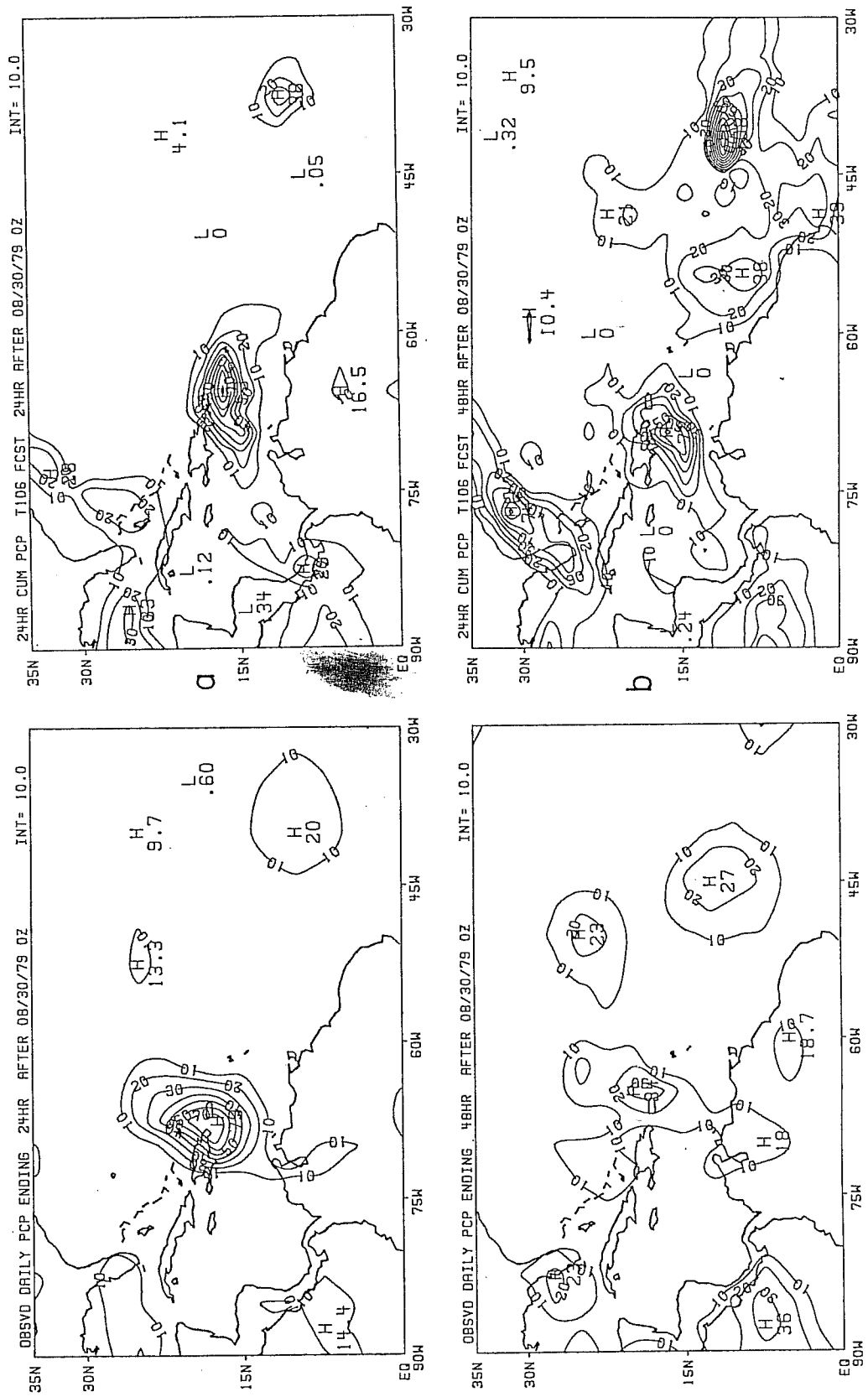
204

205

Fig. 9a, b These diagrams, respectively, show the observed (left) and the predicted (right) precipitation totals, mm/day, for hours 0 to 24 and 24 to 48.

206

7.   TYPHOON RAINFALL

Here we shall illustrate the prediction of the rainfall rates as a function of resolution for typhoon Hope. The details of the typhoon prediction are given in Krishnamurti and Oosterhof (1989). At the T170 resolution, a reasonable structure, phase and wind speed were predicted through the life cycle of the supertyphoon. This forecast degraded as the resolution was decreased to T106, T63, T42, T31 and T21.

There was a marked difference in the structure of the supertyphoon between the resolution T170 and T106. The track prediction is illustrated in fig. 10. Here we show the observed best fit track, the track from the multilevel global model at resolution T21 and T170. Also shown here is a track from a vertically integrated spectral shallow water model. Basically the best results on track forecasts came from the multilevel physical model at the highest resolution. For further details, reference should be made to Krishnamurti and Oosterhof (1989).

The dependence of maximum 24 hourly rainfall (between hours 48 to 72) as a function of spectral resolution is shown in fig. 11a. Rainfall rates show a marked increase with resolution. This illustration covers the period of the most intense development of the storm. A geographical distribution of the maximum rainfall (between hours 48 to 72) is shown in fig. 11b. In this illustration the intervals of analysis vary from 10 mm/day for T21 to 100 mm/day for T170. A dramatic increase in the rainfall occurs as the resolution is increased from T106 to T170. Between hours 48 and 72 when the supertyphoon formed the maximum rainfall for the resolution T106 was around 260 mm/day; while at T170 the rainfall amounts approached 460 mm/day. With this increased rainfall, the storm circulations increased in intensity and approached the observed supertyphoon intensities by day 5. In contrast, the maximum rainfall at the resolution T21 was around 24 mm/day between 48 and 72 hours. The sequence of 24 hour predicted rainfall for the T170 forecast is shown in fig. 12. This contains the sum of the convective and nonconvective components.

While the maximum value of condensation heating increases rapidly with the increase of horizontal resolution, the amplitude of the radiative cooling in the storm environment increases only slightly. The differential heating between the storm rain area and its environment increases rapidly with resolution. That results in a rapid growth of the divergent circulation with resolution. The divergent kinetic energy is rapidly transferred to rotational kinetic energy, i.e. the azimuthal circulation of the storm.

Figs. 13a and b show the rate of transfer of divergent kinetic energy to the rotational
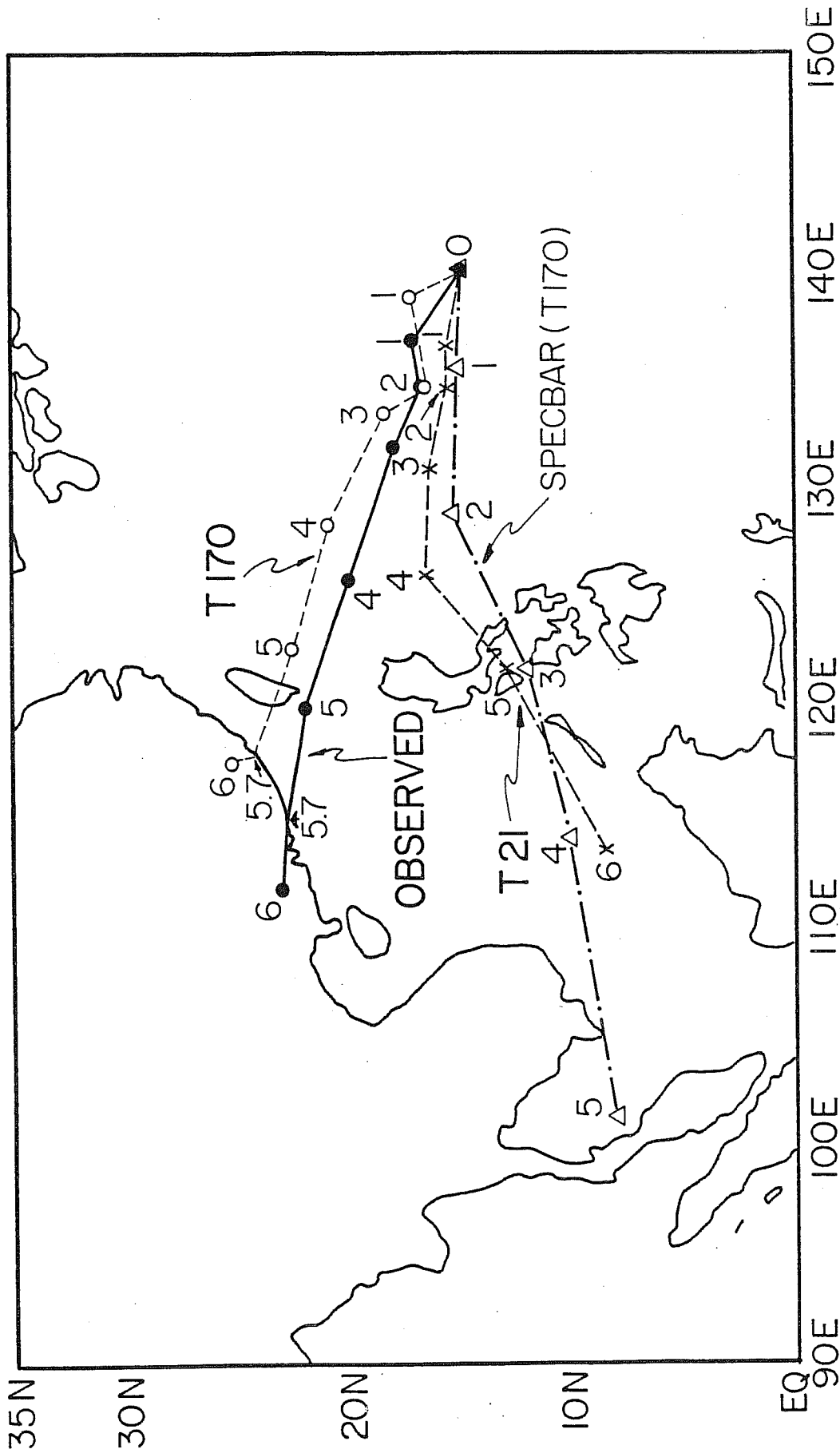
Fig. 10 Barotropic (T170) and spectral (T170, T21) forecasts are compared with the best fit tracks. Days of forecast are indicated on the side of the tracks.
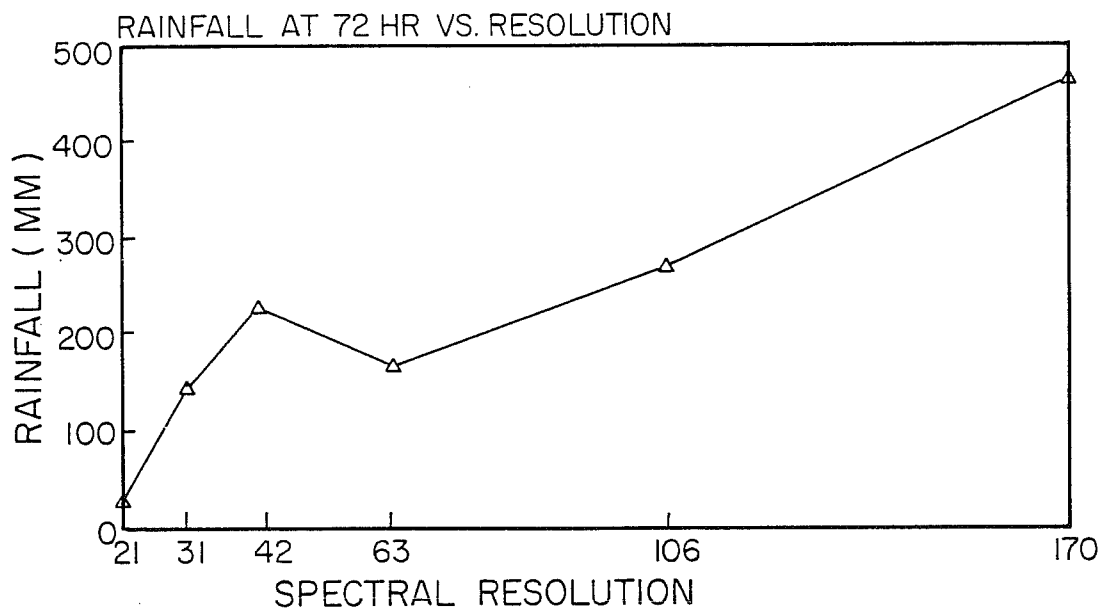
Fig. 11a Maximum rainfall amount between hours 48 and 72 as a function of resolution.
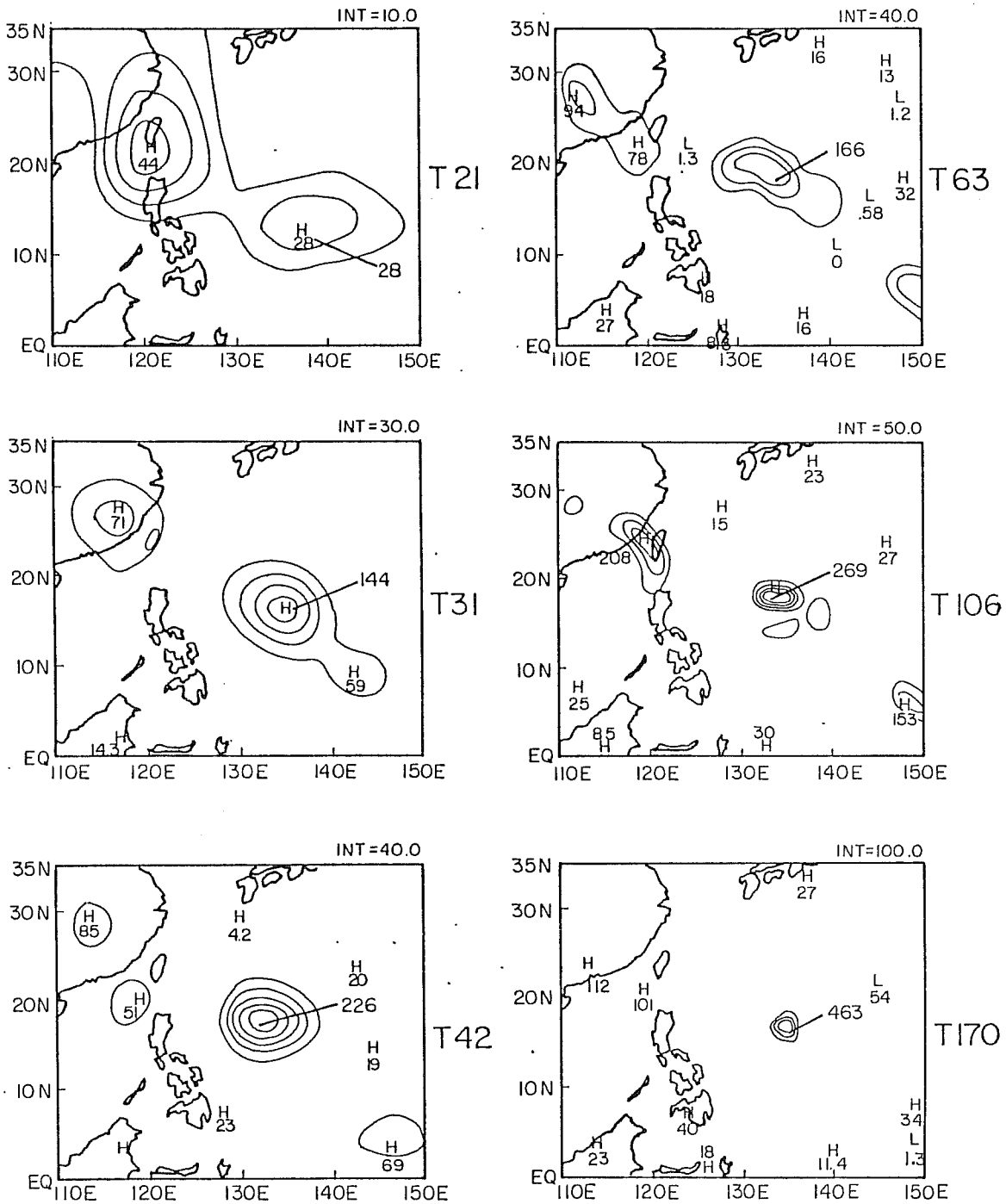
Fig. 11b Geographic distribution of rainfall accumulated between 48 and 72 hours.
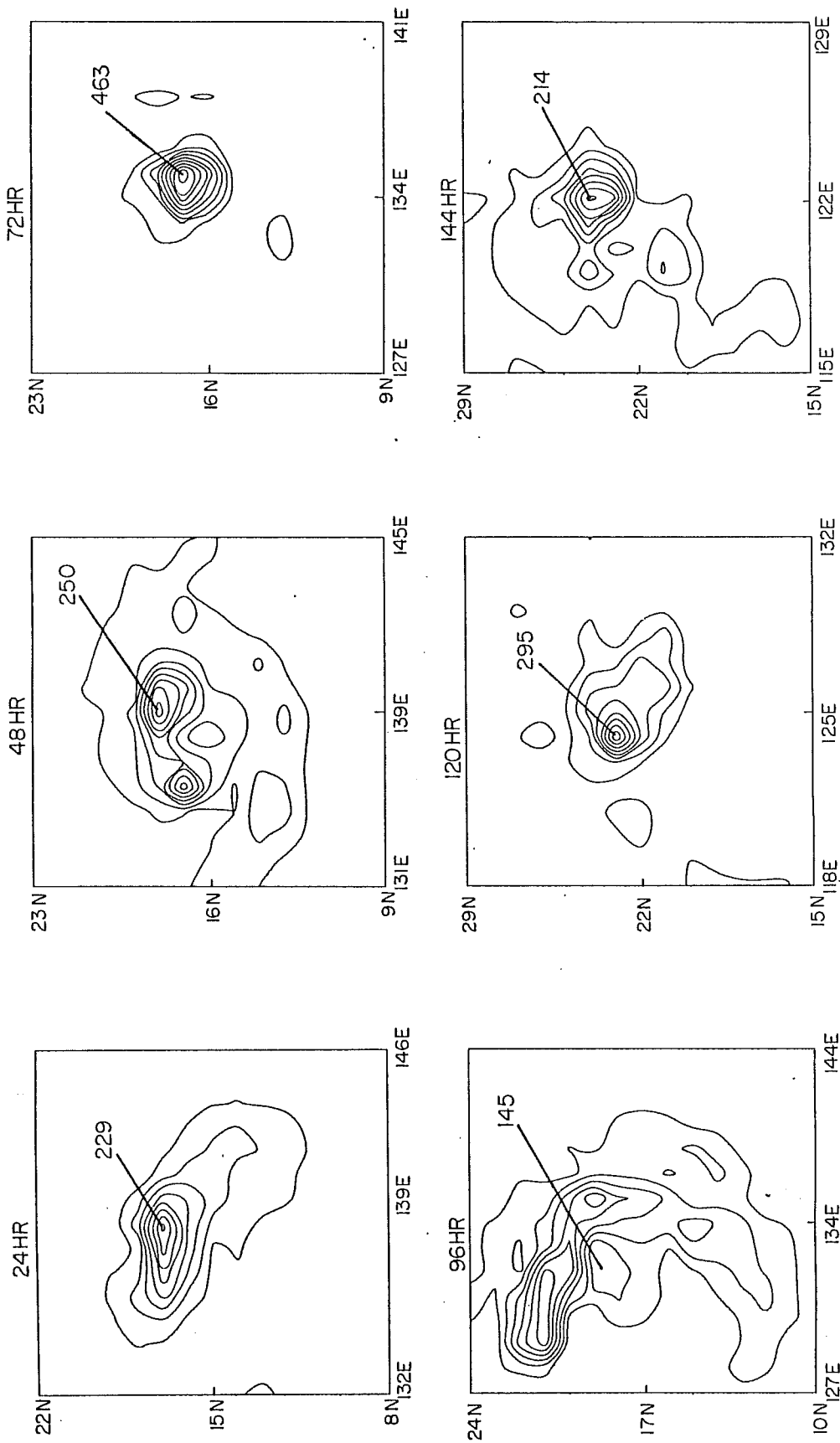
Fig. 12 Predicted rainfall fields (T170) for hours 0–24, 24–48, 48–72, 72–96, 96–120, 120–144. Units mm/day. The color scheme is explained by the scale. THe maximum rainfall between hours 48–72 is around 460 mm/day.
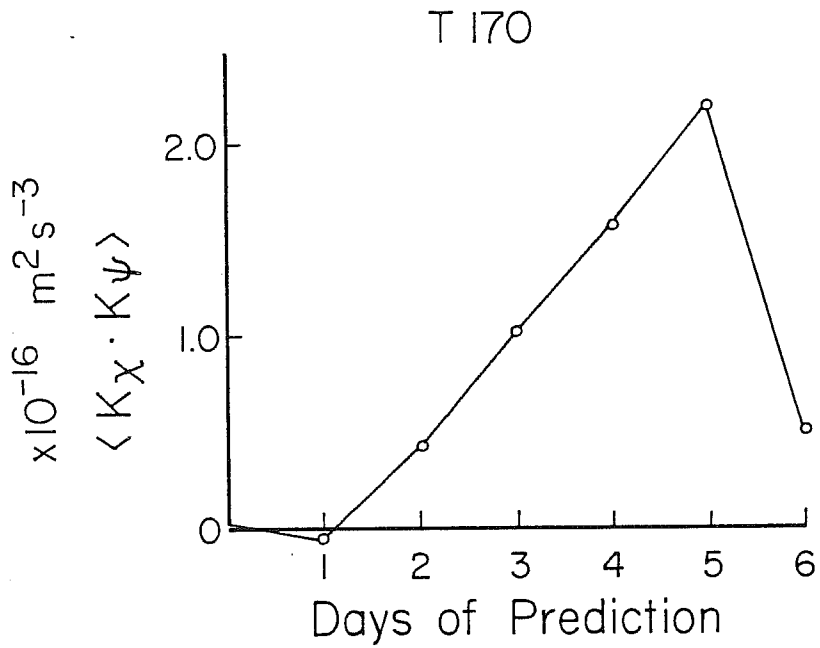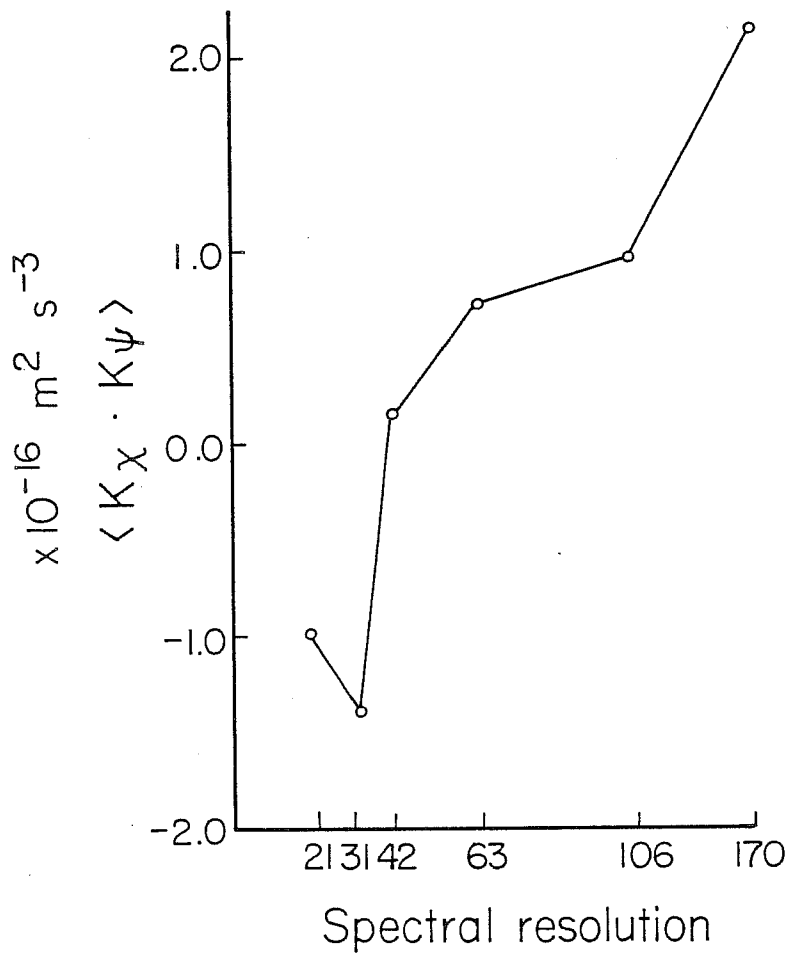
Fig. 13a Energy exchange from divergent to rotational kinetic energy for T170 storm at day 0, 1, 2, 3, 4, 5, 6.

Fig. 13b Energy exchange from divergent to rotational kinetic energy as a function of spectral resolution at day 5.

kinetic energy on day 5 when the storm had its deepest pressure and strongest intensity. These two panels, respectively, show: a) this energy exchange at the resolution T170 during the life cycle and b) as a function of spectral resolutions for day 5. The calculations of the energy exchanges shown here cover a 10° latitude/longitude square centered on the storm and the computations procedure follows Krishnamurti and Ramanathan (1982).

The storm intensity, track and structure are quite sensitive to cumulus parameterization. We have noted a major deterioration of these features as the model physics (especially the cumulus parameterization) is degraded. We feel that the present model has improved considerably in describing the entire life cycle of a supertyphoon — i.e., from the depression stage to its eventual landfall when it is weakened.

8. CONCLUDING REMARKS

We have presented a brief review on the rainfall prediction with the FSU global model at different resolutions. The lack of reliable observational estimates of rainfall (especially over oceans) is a problem that will hopefully be faced with the microwave satellite technology of the next decade. The model needs to address the cumulus parameterization more critically than has been done in the past. The global cumulus parameterization was derived from the FGGE data sets for a resolution T42. The resolution dependence of cumulus parameterization requires further observational field projects. Results thus far have used the ECMWF's FGGE IIIb data base. Experiments based on these data sets suggest that rainfall prediction, up to about 5 or 6 days, over certain regions of the tropics, seems quite promising. With further improvements in data coverage and analysis procedures much further improvement in precipitation prediction can be expected in the coming decades.

9. ACKNOWLEDGEMENTS

Appendix I
BRIEF OUTLINE OF THE GLOBAL SPECTRAL MODEL

The current tests on the cumulus parameterization were carried out on the FSU global spectral model which includes the following features:

(a) Independent variables: (x, y, σ, t).

(b) Dependent variables: vorticity, divergence, surface pressure, vertical velocity, temperature and humidity.

(c) Horizontal resolution: Triangular 21, 31, 42, 63, 106 and 170 waves.

(d) Vertical resolution: 12 layers between roughly 100 and 1000 mb.

(e) Semi–implicit time differencing scheme.

(f) Envelope orography (Wallace *et al.*, 1983).

(g) Centered differences in the vertical for all variables except humidity which is handled by an upstream differencing scheme.

(h) Fourth–order horizontal diffusion (Kanamitsu *et al.*, 1983).

(i) Kuo–type cumulus parameterization (Kuo 1965, 1974; Krishnamurti *et al.*, 1983b, 1988).

(j) Shallow convection (Tiedtke, 1984).

(k) Dry convective adjustment.

(l) Large scale condensation (Kanamitsu, 1975).

(m) Surface fluxes via similarity theory (Businger *et al.*, 1971).

(n) Vertical distribution of fluxes utilizing diffusive formulation where the exchange coefficients are functions of the Richardson number (Louis, 1981).

(o) Long– and shortwave radiative fluxes based on the band models (Harshvardhan and Corsetti 1984; Lacis and Hansen 1974).

(p) Diurnal cycle.

(q) Parameterization of low, middle and high clouds based on threshold relative humidity for radiative transfer calculations.

(r) Surface energy balance coupled to the similarity theory (Krishnamurti *et al.*, 1987).

(s) Physical initialization (Krishnamurti *et al.*, 1984).

(t) Dynamic normal mode initialization (Sugi, 1986).

Appendix II
CUMULUS PARAMETERIZATION

Following Krishnamurti *et al.* (1983b, 1988) we shall define large–scale moisture supply by the expression,

$$I_L = \frac{1}{g} \int_{P_B}^{P_T} \omega \frac{\partial q}{\partial p} \, dp. \tag{1}$$

We shall next introduce mesoscale convergence by η, so that the total supply of moisture is expressed by,

$$I = I_L(1+\eta). \tag{2}$$

The maximum amount of moisture supply, following Kuo (1965) to produce a grid square cloud is expressed by

$$Q = Q_q + Q_\theta \tag{3}$$

$$= \frac{1}{g} \int_{P_T}^{P_B} \frac{q_s - q}{\Delta \tau} \, dp$$

$$+ \frac{1}{g} \int_{P_T}^{P_B} \left[\frac{C_p T(\theta_s - \theta)}{L\theta\Delta\tau} + \omega \frac{C_p T}{L\theta} \frac{\partial \theta}{\partial p} \right] dp \tag{4}$$

The above two terms respectively denote the supply needed for moistening and heating of a unit column extending from cloud bottom (P_B) to cloud top (P_T).

We next introduce a moistening parameter b following Kuo (1974). The rainfall rate R and the total moistening M are expressed by the relations:

$$R = I(1 - b) = I_L(1 + \eta)(1 - b) \tag{5}$$

$$M = Ib = I_L(1 + \eta)b \tag{6}$$

We shall next introduce two parameters a_θ and a_q by the relation,

$$a_\theta = \frac{I(1 - b)}{Q_\theta} = \frac{I_L(1 + \eta)(1 - b)}{Q_\theta} \tag{7}$$

$$a_q = \frac{Ib}{Q_q} = \frac{I_L(1 + \eta)b}{Q_q}. \tag{8}$$

The first law of thermodynamics and the moisture conservation are expressed by

$$\frac{\partial \theta}{\partial t} = V \cdot \nabla\theta + \omega \frac{\partial \theta}{\partial p} = -\frac{1}{C_p} \left[\frac{p_0}{p} \right]^{R/C_p} H_c \tag{9}$$

$$\frac{\partial q}{\partial t} + V \cdot \nabla q + \omega \frac{\partial q}{\partial p} = E - R, \tag{10}$$

where H_c denotes heating by deep convection, the other forms of heating are not considered for the present. The R is rainfall rate and E the surface evaporation rate.

Following Krishnamurti *et al.* (1983b), we shall next express the above two equations using a_θ and a_q in the form,

$$\frac{\partial \theta}{\partial t} = V \cdot \nabla \theta + \omega \frac{\partial \theta}{\partial p} = a_\theta \left[\frac{\theta_s - \theta}{\Delta \tau} + \omega \frac{\partial \theta}{\partial p} \right] \qquad (11)$$

$$\frac{\partial \theta}{\partial t} = V \cdot \nabla_q = a_q \left[\frac{q_s - q}{\Delta \tau} \right] . \qquad (12)$$

Thus far the parameterization is not closed since we still have two unknowns namely b and η (or a_θ and a_q). We shall next write down expressions for the apparent heat source Q_1 and the apparent moisture sink Q_2 in terms of the proposed modification of the scheme of Kuo.

$$Q_1 = \frac{\partial \overline{S}}{\partial t} + \overline{V} \cdot \nabla \overline{S} + \overline{\omega} \frac{\partial \overline{S}}{\partial p} \qquad (13)$$

$$= a_\theta \left[C_p \frac{T}{\theta} \frac{(\theta_s - \theta)}{\Delta \tau} + \omega C_p \frac{T}{\theta} \frac{\partial \theta}{\partial p} \right] + C_p \frac{T}{\theta} H_R \qquad (14)$$

$$Q_2 = -L \left[\frac{\partial \overline{q}}{\partial t} + \overline{V} \cdot \nabla \overline{q} + \overline{\omega} \frac{\partial \overline{q}}{\partial p} \right] \qquad (15)$$

$$= -L \left[a_q \frac{q_s - q}{\Delta \tau} - \overline{\omega} \frac{\partial \overline{q}}{\partial p} \right] . \qquad (16)$$

Here H_R denotes the radiative heating. The two unknowns a_θ and a_q are related to the apparent heat source and the moisture sink via the relations

$$a_\theta = \frac{\overline{Q}_1 \frac{(P_B - P_T)}{g} - \frac{C_p}{g} \int_{P_T}^{P_B} \frac{T}{\theta} H_R \, dp}{\frac{1}{g} \int_{P_T}^{P_B} C_p \frac{T}{\theta} \left[\frac{\theta_s - \theta}{\Delta \tau} + \omega \frac{\partial \theta}{\partial p} \right]} \qquad (17)$$

$$a_q = \frac{\frac{\overline{Q}_2}{L} \frac{(P_B - P_T)}{g} + \frac{1}{g} \int_{P_T}^{P_B} \frac{\partial q}{\partial p}}{\frac{1}{g} \int_{P_T}^{P_B} \frac{q_s - q}{\Delta \tau}} \qquad (18)$$

where $\overline{Q}_1$, $\overline{Q}_2$ denote the vertical averages of Q_1, Q_2 between P_T and P_B. At this stage we shall introduce nondimensional net moistening and rainfall by the relations

216

$$\frac{M}{I_L} = \frac{(Q_2/L + I_L)}{I_L} \qquad\qquad (19)$$

$$\frac{R}{I_L} = \frac{\bar{Q}_1 - C_p T/\theta \bar{H}_R}{I_L} . \qquad\qquad (20)$$

We now make use of atmospheric observations to define a closure for the two unknowns using a multiple regression approach. The previous study was based on GATE observations where the time series of M/I_L and R/I_L were first constructed from the GATE A/B scale ship array of data. These series were next subjected to a multiple screening regression with respect to the time series of several large–scale variables. Among these, the 700 mb relative vorticity and the vertically integrated vertical velocity $\bar{\omega}$ appeared the most important. Thus we express the vertically integrated moistening and heating rates by the regression equations,

$$\frac{M}{I_L} = a_1\zeta + b_1\bar{\omega} + c_1 \qquad\qquad (21)$$

$$\frac{R}{I_L} = a_2\zeta + b_2\bar{\omega} + c_2 . \qquad\qquad (22)$$

It is easy to see that the closure of the scheme (based on ζ, $\bar{\omega}$) yields values for any of the following pairs: (M, R); (Q_1, Q_2); (a_θ, a_q); (b, η). The aforementioned calculations are carried out on the sigma surfaces ($\sigma = p/p_s$) in a 12–layer spectral model.

Here ζ denotes the relative vorticity at the $\sigma = 0.7$ surface. The vertically averaged $\bar{\omega}$ is from $\sigma = 0.1$ to $\sigma = 1.0$, where ω is determined from $\dot{\sigma}$ by relation,

$$\frac{\omega}{p_s} = \dot{\sigma} + \sigma \left[\frac{\partial \ln p_s}{\partial t} + V \cdot \nabla \ln p_s\right].$$

It should be noted that in these regression equations the rainfall rate R and the moistening rate M are functions of three variables, i.e. I_L ζ and $\bar{\omega}$. In the present study the formulation of the problem remain essentially the same, except that we shall estimate a global (tropical) rather than a regional (GATE) regression. Thus in the present study the coefficients of multiple regression a_1, b_1 a_2, b_2 and c_2 vary geographically. For this study we utilized global FGGE IIIb analysis as a data base. The use of GATE observations in the previous study had the advantage that high quality observations, uncontaminated by excessive analysis, provided the statistical correction for the Kuo type cumulus parameterization. Although the FGGE IIIb analysis is based on the best available global observations, it is not the same quality of time series data set as GATE over many regions. However, the premise of the present study is that the global statistical correction to the scheme of Kuo may provide a better description and prediction of the tropical

precipitation and the convective process in comparison to an application of the GATE findings. Furthermore heavy precipitation rates in excess of 35 mm day^{-1} are not being handled by the previous scheme (Krishnamurti et al., 1983b) due to the upper limit of the

GATE histories. The limits of ζ and $\bar{\omega}$ outside GATE area in the previous scheme were restricted within the extremes observed during the GATE. This was necessary as the regression equations were derived using parameters within these limits. This restricted the tropical rainfall amounts predicted by this scheme to about 35 mm/day consistent with GATE histories. That limitation is considerably relaxed by the global data sets of precipitation in the proposed regression. The heavy orographic precipitation is another area that is being handled in the present context.

The requirement for an additional moisture amount ηI_L over a vertical column requires that we remove an equivalent amount somewhere for moisture conservation. In the present formulation that is executed mostly in the boundary layer. We require that

$$\frac{1}{(g\Delta t)} \int_0^1 (q^* - q)d\sigma = \eta I_L \tag{23}$$

where q^* is a modified specific humidity and δt is the time step. By setting $q^* = \varepsilon q$, where q is largest i.e. the planetary boundary layer. Thus,

$$\varepsilon = 1 + \eta I_L / \frac{1}{(g\Delta t)} \int_{0.1}^1 q d\sigma \tag{24}$$

$$q^* = q[1 + \eta I_L / \frac{1}{(g\Delta t)} \int_{0.1}^1 q d\sigma] \tag{25}$$

This parameterization is structured to the FSU global spectral model.

References

Arkin, P.A., A.V.R. Krishna Rao and R.R. Kelkar, 1989: Large–Scale Precipitation and Outgoing Longwave Radiation from INSAT–1B during the 1986 Southwest Monsoon Season. *Journal of Climate*, 2, 619–628.

Bengttson, L. and J. Shukla, 1988: Integration of Space and In Situ Observations to Study Global Climate Change. *Bulletin of the American Meteorological Society*, 69, 1130–1143.

Businger, J.A., J.C. Wyngard, Y, Izumi and E.F. Bradley, 1971: Flux profile relationship in the atmospheric surface layer. *J. Atmos. Sci.*, 28, 181–189.

Dastoor, A. and T.N. Krishnamurti, 1989: Impact of resolution and ground wetness parameterization on the prediction of the landfall of a tropical cyclone. To be published in *Boundary Layer Meteorology*.

Harshvardhan, and T.G. Corsetti, 1984: Longwave parameterization for the UCLA/GLAS GCM. NASA Tech. Mem. 86072. (Available from Goddard Space Flight Center, Greenbelt, MD.)

Kanamitsu, M., K. Tada, K. Kudo, N. Sato and S. Isa, 1983: Description of the JMA operational spectral model. *J. Met. Soc. Japan*, 61, 812–828.

Kanamitsu, M., 1975: On numerical prediction over a global tropical belt. Report No. 75–1, Dept. of Meteorology, Florida State University, Tallahassee, Florida 32306, pp. 1–282.

Krishnamurti, T.N. and Y. Ramanathan, 1982: Sensitivity of monsoon onset of differential heating. *J. Atmos. Sci.*, 39, 1290–1306.

Krishnamurti, T.N., S. Cocke, R. Pasch and S. Low–Nam, 1983a: Precipitation estimates for raingauge and satellite observations. Florida State University Report No. 83–7, Department of Meteorology, Florida State University, Tallahassee, Florida 32306, pp. 1–373.

Krishnamurti, T.N., S. Low–Nam and R. Pasch, 1983b: Cumulus parameterization and rainfall rates II. *Mon. Wea. Rev.*, 111, 816–828.

Krishnamurti, T.N., K. Ingles, S. Cocke, T. Kitade and R. Pasch, 1984: Details of low latitude medium range numerical weather prediction using a global spectral model. Part II: Effects of orography and physical initialization. *J. Meteor. Soc. Japan*, 62, 613–649.

Krishnamurti, T.N., S. Low–Nam, A. Kumar, J. Sheng, and M. Sugi, 1987: Numerical Weather Prediction of Monsoons, Monsoon Meteorology, Oxford University Press.

Krishnamurti, T.N. and H.S. Bedi, 1988: Cumulus Parameterization and Rainfall Rates III. *Mon. Wea. Rev.*, 116, 583–599.

Krishnamurti, T.N. and D. Oosterhof, 1989: Prediction of the life cycle of a supertyphoon with a high resolution global model. To be published in the October issue of the *Bulletin of the American Meteorological Society*.

Krishnamurti, T.N., D. Oosterhof and N. Dignon, 1989a: Hurricane Prediction with a High Resolution Global Model. *Mon. Wea. Rev.*, 117, 631–669.

Krishnamurti, T.N., A. Kumar, K.S. Yap, A.P. Dastoor, N. Davidson, and J. Sheng, 1989b: Performance of a high resolution meso–scale tropical prediction model. To be published in the October issue of *Advances in Geophysics*.

Kuo, H.L., 1965: On formation and intensification of tropical cyclones through latent heat release by cumulus convection. *J. Atmos. Sci.*, 22, 40–63.

Kuo, H.L., 1974: Further studies of the parameterization of the influence of cumulus convection on large scale flow. *J. Atmos. Sci.*, 31, 1232–1240.

Lacis, A.A. and J.E. Hansen, 1974: A parameterization for the absorption of solar radiation in the earth's atmosphere. *J. Atmos. Sci.*, 31, 118–133.

Louis, Jean–Francois, 1981: A parametric model of vertical eddy fluxes in the atmosphere. *Boundary Layer Meteorology*, 17, 187–202.

Luo, H. and M. Yanai, 1984: The large–scale circulation and heat sources over the Tibetan Plateau and surrounding areas during the early summer of 1979. Part II: Heat and moisture budgets. *Mon. Wea. Rev.*, 112, 966–989.

Manobianco, John, 1988: On the Observational and Numerical Aspects of Explosive East Coast Cyclogenesis. Ph.D. Dissertation. (Available from the Department of Meteorology, The Florida State University, Tallahassee, Florida 32306, USA.)

Martin, David W., 1983: Measuring Rainfall, from Space. Proceedings of CCNAA–AIT Joint seminar on Monsoon and Tropical Meteorology, April 17–22, 157–162. (Available from the Taiwan Meteorological Society, Taipei, Taiwan.)

Pasch, R.J., 1983: On the onset of the planetary scale monsoon. FSU Rep. No. 83–91, 187 pp. [Available from the Dept. of Meteorology, Florida State University, Tallahassee, Florida 32306, USA.]

Reed, R.J., E. Klinker and A. Hollingsworth, 1987: An Evaluation of the performance of the ECMWF operational forecasting system in analysing and forecasting tropical easterly wave disturbances. Part II: Spectral Investigation. Technical Report No. 60. (Available from the European Centre for Medium Range Weather Forecasts, Shinfield Park, Reading, Berkshire, RG2 9AX, England.)

Reed, R.J., A. Hollingsworth, W.A. Heckley and F. Delsol, 1988: An evaluation of the performance of the ECMWF operational system in analyzing and forecasting tropical easterly wave disturbances over Africa and the Tropical Atlantic. *Mon. Wea. Rev.*, 116, 824–865.

Sugi, M., 1986: Dynamic Normal Mode Initialization, *J. Meteor. Soc. Japan*, 5, 623–636.

Tiedtke, M., 1984: The sensitivity of the time–mean large–scale flow to cumulus convection in the ECMWF model. Workshop on convection in large–scale numerical models. ECMWF, 28 Nov. – 1 Dec. 1983, 297–316.

Wallace, J.M., S. Tibaldi and A.J. Simmons, 1983: Reduction of systematic forecast errors in the ECMWF model through the introduction of envelope orography. *Quart. J. Roy. Met. Soc.*, 109, 683–718.

Yanai, M., S. Esbensen and J.H. Chu, 1973: Determination of bulk properties of tropical cloud clusters from large–scale heat and moisture budgets. *J. Atmos. Sci.*, 30, 611–627.